Liu *et al. Collagen and Leather* (2024) 6:13
https://doi.org/10.1186/s42825-024-00156-8

Collagen and Leather

RESEARCH

Open Access

Therapeutic potential of gelatine methacrylate hydrogels loaded with macrophage-derived exosomes for accelerating angiogenesis and cutaneous wound healing

Jiajun Liu[1], Fuying Chen[1], Luoqiang Tian[1], Jinjie Wu[2], Keting Liu[1], Qiwen Wan[1], Bo Yuan[1], Xiangdong Zhu[1], Xuening Chen[1*] and Xingdong Zhang[1]

Abstract

Extensive studies demonstrate that macrophage response plays an important role in regulating angiogenesis via a paracrine way, which is crucial for skin wound repair. This study isolated and characterized nanosized exosomes from differently polarized macrophages (MΦ), including M0 (naïve), M1 (pro-inflammatory), and M2 (anti-inflammatory) macrophages, and further assessed their impacts on angiogenesis and skin regeneration. Our results indicated that compared to M0 and M1 counterparts, M2 macrophage-derived exosomes (M2-Exos) exhibited a pronounced ability to promote angiogenic ability of of human umbilical vein endothelial cells (HUVECs) by enhancing expression of angiogenic genes and proteins, increasing cell migration, and improving tubulogenesis. Bioinformatics analyses suggested that the distinct angiogenic potentials of three MΦ-Exos might be attributed to the differentially expressed angiogenesis-related miRNAs and their target genes such as Stat3, Smad 2, and Smad4. Moreover, these isolated MΦ-Exos were integrated with gelatine methacrylate (GelMA) hydrogels to achieve the sustained delivery at murine full-thickness cutaneous wound sites. In vivo results showed that Gel/M2-Exos significantly augmented angiogenesis, accelerated re-epithelialization, promoted collagen maturity, thereby promoting wound healing. In contrary, Gel/M1-Exos showed the opposite effects. Our findings provided compelling evidence that the polarization status of macrophages significantly affected angiogenesis and wound healing via the miRNA cargos of their derived exosomes. Moreover, this study opens a new avenue for developing nano-scale, cell-free exosome-based therapies in treating cutaneous wounds.

Keywords Exosomes, Angiogenesis, Wound healing, Macrophage polarization, Gelatine methacrylate

*Correspondence:
Xuening Chen
xchen6@scu.edu.cn
Full list of author information is available at the end of the article

Graphical abstract

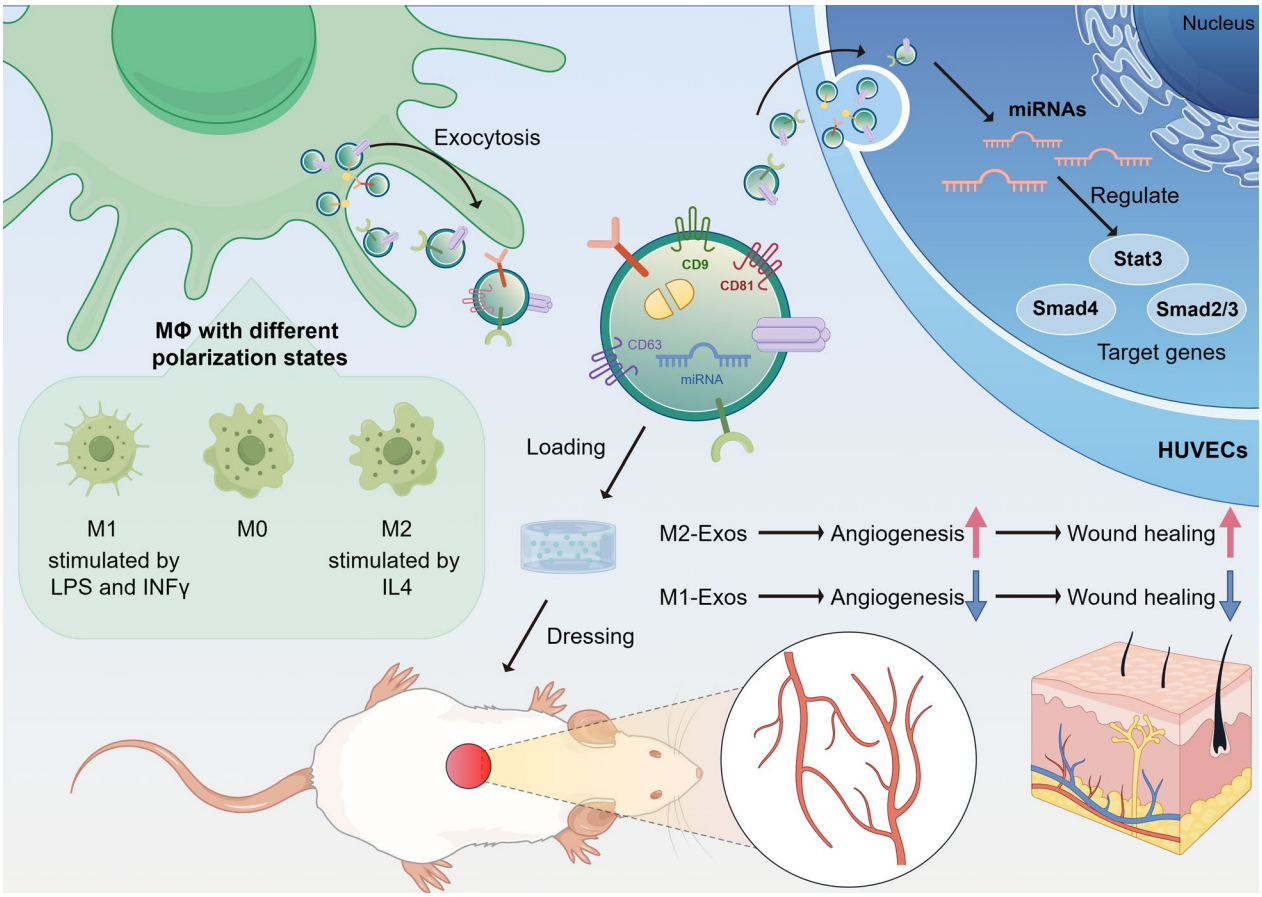

1 Introduction

As the largest organ of human body, the skin is often damaged by disease, burn, accidental trauma, surgical procedures, and so on [1, 2]. The delayed healing of cutaneous wounds compromise skin integrity, leading to infections and scars [3]. Therefore, it is urgent to shorten the wound healing time, and restore its structural integrity and function after skin injury in clinics.

Wound healing is a complex biological process involving hemostasis, inflammation, proliferation (granulation), and remodeling [4]. Central to this process is angiogenesis, the formation of new blood vessels, which is essential for delivering oxygen and nutrients to the wound site, thereby facilitating tissue repair and regeneration [5, 6]. The efficiency of angiogenesis significantly influences the duration and outcome of wound healing [7]. It suggests that therapeutic strategies aimed at enhancing angiogenesis may be a feasible approach to prevent scar formation and promote skin repair.

Recent research has demonstrated the pivotal role of inflammation, particularly the response of macrophages, in the regulation of angiogenesis [8, 9]. Macrophages, as one of the dominant immune cells, exhibit remarkable plasticity. Macrophage in a resting state is often referred to as M0 phenotype, which can be polarize into distinct phenotypes under different stimuli, including two extremes as classically activated M1 phenotype, and alternatively activated M2 phenotype [10, 11]. The pro-inflammatory M1 macrophages induced by lipopolysaccharides (LPS) and interferon-γ (IFN-γ) often secrete inflammatory cytokines such as interleukin (IL)-1β, inducible nitric oxide synthase (iNOS), tumor necrosis factor (TNF)-α to aggravate inflammation. The anti-inflammatory M2 macrophages induced by IL-4 often highly express anti-inflammatory mediators such as IL-10 and arginase-1 (ARG) to reduce inflammation and promote tissue regeneration [12]. The balance between these phenotypes influences the inflammatory environment

and, consequently, the angiogenic process, making the modulation of macrophage activity a potential therapeutic target for improving wound healing[13].

Exosomes (Exos), small membrane-bound vesicles, have emerged as key players in cell-to-cell communication, capable of influencing recipient cell behaviors and tissue regeneration[14, 15]. Derived from various cell types, including macrophages, exosomes transport proteins and genetic materials such as mRNAs, miRNAs, and other non-coding RNAs, potentially regulating angiogenesis during wound healing. However, the specific effects of exosomes from differently polarized macrophages (MΦ-Exos) on angiogenesis and the underlying mechanisms remain to be fully elucidated[16–22].

There is a big challenge in achieving sustained delivery of exosomes and maintaining their therapeutic activity at wound sites. Due to its 3D aqueous porous structure, good biocompatibility, and tunable mechanical properties, Gelatin methacryloyl (GelMA) hydrogel emerges as an potential carrier[23]. Recently, Isik et al. [24]loaded GelMA hydrogels with human periodontal ligament stem cells-derived exosomes to promote the rat calvarial defect regeneration. Zhao et al.[25], combined GelMA hydrogel with human umbilical vein endothelial cells (HUVECs) -derived exosomes to repair full-thickness cutaneous wounds. These findings have demonstrate that GelMA hydrogel enables the encapsulation and controlled release of bioactive substances, including exosomes, to the wound site, offering a promising approach for enhancing skin regeneration.

This study aims to elucidate the angiogenic potential of exosomes derived from macrophages in different polarization states (M0, M1, M2) and to investigate the efficacy of their delivery using GelMA hydrogels in promoting cutaneous wound healing. By comparing the effects of these exosomes on endothelial cell function and wound repair, we seek to deepen our understanding of macrophage-mediated angiogenesis and open new avenues for cell-free, exosome-based therapeutic strategies in skin regeneration.

2 Materials and methods

2.1 Culture and polarization of macrophages

RAW 264.7 macrophages were obtained from Procell (Wuhan, China), and cultured in Dulbecco's modified Eagle's medium (DMEM, Servicebio, China) supplemented with 10% fetal bovine serum (FBS, Gibco, USA) and 1% penicillin–streptomycin (HyClone, USA) at 37 °C with 5% CO2 in a humidified incubator. The orginal macrophages were the resting unpolarized M0 phenotype (referred as M0). Then, the M0 macrophages were polarized to pro-inflammatory M1 phenotype (referred as M1) by using 100 ng/mL lipopolysaccharide (LPS) and 20 ng/mL interferon (INF)-γ and anti-inflammatory M2 phenotype (referred as M2) by using 40ng/mL IL-4.

2.2 Identification of polarized macrophages

2.2.1 Nitric oxide detection

Nitric oxide (NO) levels were tested in the supernatants of macrophages with different polarization status on day 1 and 2 by using a Nitric oxide detection kit (Beyotime, S0021S, China).

2.2.2 Quantitative reverse transcription PCR (qRT-PCR)

The total RNAs of three types of macrophage were isolated by using the SteadyPure Universal RNA Extraction Kit (Accurate Biology, AG21017, China) on day 2. Complementary DNA (cDNA) was synthesized by using a PrimeScript RT reagent kit (Accurate Biology, AG11706, China), and qPCR procedure was performed with CFX96TM system (Bio-Rad, USA) to measure the expression of marker genes for M1 phenotype (i.e., *iNos, Tnf, Il1, Il6*) and M2 phenotype (i.e., *Cd206, Arg*) by using a SYBR Green PCR Master Mix kit (Accurate Biology, AG11701, China). G*apdh* was used as a housekeeper gene for the result normalization. The primer sequences are listed in Additional file 1: Table S1.

2.2.3 Immunofluorescence (IF) staining for macrophage phenotype markers

On day 2, macrophages different polarization status were fixed in 4% paraformaldehyde (PFA, Biosharp, China) at room temperature (RT) for 5 min and washed with PBS three times. The cells were permeabilized with 0.1% Triton X-100 (BioFroxx, Germany) for 5 min at RT and then blocked with 5% bovine serum albumin (BSA) (BioFroxx, Germany) at 37 °C for 60 min. Then, the cells were stained with the primary antibodies for either iNOS (Cell Signaling, USA) or CD206 (Cell Signaling, USA) at 4 °C overnight, followed the incubation with fluorescence secondary antibody (Boster, China) at RT for 2 h. Finally, the nuclei were stained with DAPI (Beyotime, China) for 1 min. The images were captured by using the inverted fluorescent microscope (Leica, Germany) and analyzed with ImageJ software.

2.3 Isolation and characterization of macrophage-derived exosomes (MΦ-Exos)

2.3.1 Exosome isolation

After the macrophages were polarized under the stimulation of either LPS and INF-γ or IL-4 for 48 h, the media were replaced with DMEM (Servicebio, China) supplemented with 10% Exos-free FBS for another 48 h. Then, the MΦ-Exos of different groups were extracted by ultra-centrifugation. In brief, the supernatants of different groups were centrifuged at 300 × g at 4 °C for 5 min

and filtered through a 5 μm filter to remove the cells. The supernatant was centrifuged at 2,000×g at 4 °C for 20 min and filtered through a 1.2 μm filter to remove cell debris and large particles. After centrifuged at 12,000×g at 4 °C for 30 min, the resulting supernatant was transferred to higher-strength ultra-centrifuged tubes and ultra-centrifuged at 120,000×g at 4 °C for 90 min. All precipitates were resuspended with 10 mL of PBS and recentrifuged at 120,000×g at 4 °C for 90 min. After the supernatant was removed, the precipitates were dissolved in 50–200 μL of PBS, filtered through 0.22 μm filter, and immediately stored at − 80 °C for further study. The exosomes derived from macrophages of unpolarized M0 phenotype, M1 phenotype, and M2 phenotype were named as MΦ0-Exos, MΦ1-Exos, and MΦ2-Exos, respectivley. The concentrations of proteins in Exos were determined by BCA protein assay kit (Solarbio, China).

2.3.2 Exosome characterization

The morphology of MΦ-Exos was visualized by using transmission electron microscope (TEM). In brief, 20 μL of the fresh exosomes were loaded on carbon-coated copper electron microscopy grids for 2 min and then negatively labeled with the phosphotungstic acid solution for 5 min. The grids were washed three times with PBS to remove extra phosphotungstic acid solution and maintained under a semi-dry condition. Images were obtained by using a transmission electron microscope (TEM, JEM-2100Plus, Japan) and analyzed by using ImageJ software.

Surface marker expression and particle sizes of MΦ-Exos were characterized by using nanoflow. In brief, 1 μL of the PerCP/Cyanine5.5 anti-mouse CD9 antibody was diluted with 9 μL of PBS, and the PE anti-mouse CD63 antibody was diluted in the same way. 10 μL Exo-contained solution was added with 1 μL diluted PerCP/Cyanine5.5 anti-mouse CD9 antibody (biolegend, USA). Taking another 10 μL Exo-contained solution was added with 1 μL diluted PE anti-mouse CD63 antibody (biolegend, USA), and then incubated at 37° C in the dark for 30 min. Subsequently, the labeled MΦ-Exos were diluted to 100 times and analyzed by Flow NanoAnalyzer (Nanofcm U30, China).

2.4 Cell culture and seeding

Human umbilical vein endothelial cells (HUVECs) were obtained from the the Cell Bank of the Chinese Academy of Sciences (Shanghai, China). HUVECs were cultured in DMEM medium (Servicebio, China) supplemented with 10% FBS (Gibco, USA) and 1% penicillin/streptomycin (Gibco, USA) in the incubator with a humidified atmosphere of 5% CO_2 at 37℃. After 80–90% confluence, HUVECs were harvested and seeded in the well-plates for further analyses. The culture media were changed every two days.

2.5 Exosome labeling and uptake

The purified MΦ-Exos were labeled with PKH67 (Bestbio, China). In brief, the dye solution was prepared by adding 4 μL of PKH67 to 1 mL of diluent C. Then, exosomes were resuspended in the mixing dye solution for 5 min and then incubated in 1% BSA for 1 min to stop the staining. Labeled exosomes were ultra-centrifuged at 120,000×g for 70 min, washed with PBS, ultra-centrifuged again, and resuspended in 50 μL of PBS. PKH67-labeled exosomes derived from different polarized macrophages were incubated with HUVECs (5×10^3 cells/well) in 96-well plates at 37 °C. After 12 h, HUVECs were fixed with 4% PFA. The cytoskeleton was labeled with FITC-labeled phalloidin at room temperature for 45 min, and the nucleus was stained with 4′,6-diamidino-2-phenylindole (DAPI). The uptake of the labeled exosomes by HUVECs was determined by using the inverted fluorescent microscope (Leica, Germany).

2.6 CCK-8 assay

A Cell Counting Kit-8 assay (CCK-8, Dojindo, Japan) was used to assess cell proliferation. In brief, HUVECs (5×10^3 cells/well) were seeded onto 96-well plates, and cultured with 50 μg/mL M0-exos, M1-exos, and M2-exos at 37 °C, respectively. On day 3 and 7, the media were replaced with fresh DMEM media containing 10% CCK8, followed by incubation at 37 °C for 2 h. The absorbance was measured at 450 nm using a microplate reader (Thermo Fisher, USA). The optical density values represented the proliferation of HUVECs.

2.7 Scratch wound assay

The scratch wound assay was performed to reflect the effect of MΦ-Exos on the cell migration. In brief, HUVECs (5×10^4 cells/well) were seeded into 48-well plates until confluence. Then, the 1mL sterile micropipette tip was used to make a liner scratch wound across each well. After washed three times with PBS, each well was added fresh media containing 2% FBS and 50 μg/mL of different exosomes. Finally, the well-plates were incubated at 37 °C with 5% CO_2 and imaged by an inverted microscope at 0h, 12 h, and 24 h, respectively.

2.8 Angiogenic differentiation of HUVECs

HUVECs were co-cultured with different MΦ-Exos (50 μg/mL) in 96-well plates at a density of 5×10^3 cells/well and 48-well plates at the density of 5×10^4 cells/well.

2.8.1 IF staining for VEGF

On day 3 and 7, HUVECs were fixed with 4% PFA. Following the similar immunofluorescence (IF) staining procedures mentioned in Sect. 2.2.3, the expression of specific angiogenic protein—VEGF was measured by using rabbit anti mouse VEGF primary antibody (Hua-Bio, China) and DyLight 594 Conjugated AffiniPure Goat Anti-rabbit IgG (H + L) (Boster, China).

2.8.2 qRT-PCR for angiogenic gene expression

On day 3 and 7 day, HUVECs were collected to analyze the expression of angiogenic genes (*i.e., Vegf, Ang, Acvrl1, Fgfr, Pbdg-d, and Tgf*β), following the similar procedures mentioned in Sect. 2.2.2. The primer sequences are listed in Additional file 1: Table S1.

2.8.3 Tube formation assay

The effects of MΦ-Exos on angiogenesis was also evaluated by the tube formation assay in vitro. Briefly, 50 μL Matrigel (ABW, China) was added each well of 96-well plate and incubated at 37°C for 30 min. Then, HUVECs (4×10^4 cells/well) were seeded on the Matrigel and treated with different MΦ-Exos (50 μg/mL). Tube formation was analyzed after 6h treatment by using an inverted microscope. Tubules were photographed in 3–5 random fields per well and measured by ImageJ software.

2.9 miRNA analysis of MΦ-Exos

The loading levels of key miRNAs associated with angiogenesis in three MΦ-Exos were evaluated, including mmu-miR-125a-3p, mmu-miR-125b-5p, mmu-miR-146a-5p, mmu-miR-155-5p, mmu-miR-107-3p, mmu-miR-145a-5p, mmu-miR-150-5p, mmu-miR-19a-3p, mmu-miR-210-3p, mmu-miR-23a-3p, mmu-miR-26a-5p, mmu-miR-17-5p, mmu-miR-27b-3p, mmu-miR-21a-5p, mmu-miR-214-3p. Briefly, the total RNA of three types of exosomes (20 μg each) was isolated by using Trizol reagent (Ambion, USA), followed by cDNA synthesis of miRNA by using a miRNA cDNA first-strand synthesis kit (Accurate Biology, China). The qPCR procedure utilized the CFX96TM system from Bio-Rad (USA), with a SYBR Green PCR Master Mix kit (Accurate Biology, China). The miRNA expression was normalized by U6 and calculated as a fold difference from the control group.

To investigate the roles of the above miRNAs with significant differences, TargetScan, miRDB, and miRTarBase databases integrated in miRWalk (http://mirwalk.umm.uni-heidelberg.de) were used to predict their target genes, in which the number of predicted target genes were 1584, 2076 and 1031, respectively. As shown in Fig. 5b, 387 target genes were identified by using Venny 2.1.0 for the intersection analysis of three databases. Then, Kyoto Encyclopedia of Genes and Genome (KEGG) and Gene ontology (GO) analyses of DEGs were performed by using the Database for Annotation Visualization and Integrated Discovery (DAVID) [26]. A protein–protein interaction (PPI) network map was created by using the STRING database. The top 10 hub genes were also identified through the Maximum Correlation Criteria of the cytoHubba plugin in Cytoscape v3.8.0.

2.10 Preparation and characterization of GelMA hydrogels loaded with MΦ-Exos

Following the similar procedure mentioned before[27], GelMA macromers were synthesized and thoroughly dissolved in PBS to achieve a concentration of 15 wt%. 30 μL of 10 mg/ml of photoinitiator lithium phenyl-2,4,6-trimethylbenzoylphosphinate (LAP, Stem Easy, China) solution was added into every 1 mL of GelMA solution. Then, GelMA hydrogel was prepared by transferring 100 μL of the mixed solution into a customized polytetrafluoroethylene (PTFE) cylindrical mold (8 mm in diameter, 2 mm in height), and exposed to 405 nm ultraviolet light (EFL, China) for 1 min at a distance of 5 cm to initiate the gelation process. Moreover, exosome-loaded GelMA hydrogels were prepared by adding 50 μg of three pre-isolated MΦ-Exos into 100 μL of the mixed solution before gelation, named as Gel/M0-exos, Gel/M1-exos, and Gel/M2-exos, respectively.

The rheological properties of GelMA hydrogel and MΦ-Exos-loaded GelMA hydrogels were measured by using the rheometer (Anton Paar, Austria). After freeze-dried, the cross-sectional surface of these hydrogels was visualized by using a field emission scanning electron microscope (FE-SEM, JSE-5900LV, Japan). To detect the distribution of exosomes in GelMA, MΦ-Exos were labeled with DiL (Beyotime, China), and then observed by using a Confocal laser scanning microscope (CLSM,Carl zeiss, Germany). The release capability of MΦ-Exos-loaded GelMA hydrogels was assessed by identifying the exosomes released into the PBS solution via a BCA protein assay kit.

2.11 In vivo wound healing study

The animal experiment was approved by Institutional Animal Care and Use Committee at Sichuan University (Chengdu, China), and the surgery was performed according to the Guide for the Care and Use of Laboratory Animals published by the National Academy of Sciences, China. BALB/c mice (20-25 g, 8-week-old) were anesthetized by intraperitoneal injection of 4% chloral hydrate (10 mL/kg), and full-thickness skin wounds of 8 mm in diameter were created on the center of their backs. Thirty-two mice were used and randomly divided into four groups, including (1) GelMA group, the wounds

were covered by pure GelMA; (2) Gel/M0-exos group, the wounds were covered by GelMA loaded with 50 μg M0-Exos; (3) Gel/M1-exos group, the wounds were covered by GelMA loaded with 50 μg M1-Exos; (4) Gel/M2-exos group, the wounds were covered by GelMA loaded with 50 μg M2-Exos. The wound areas were photographed on 0, 3, 5, 7, 10 and 14 days after surgery, and the wound areas were measured by using ImageJ software. On day 7 and 14 after surgery, four mice in each group were sacrificed for further analysis. The subcutaneous angiogenesis in the wound sites was also photographed.

2.12 Histological analysis and immunostaining

On day 7 and 14, the samples were harvested, fixed with 4% PFA, dehydrated gradually by a series of graded ethanol solution, and embedded in paraffin. Then, the embedded specimens were cut vertically into serial sections with 5 μm thickness. For histological analysis, the sections were stained with hematoxylin and eosin (H&E) (Biosharp, China) and Masson's trichrome staining (Servicebio, China). Moreover, immumohistochemical (IHC) staining of type I and III collagen (Col I and Col III) was performed to evaluate the wound repair, following the similar procedure mentioned before [28]. The sections were incubated with primary antibodies against collagen I (1:1000, Servicebio, China) and Collagen III primary antibody (1:500, Servicebio, China) at 4 °C overnight, and treated with HRP conjugated goat anti-rabbit IgG (1:200, Servicebio, China) for 1h at room temperature. The stained slices were scanned under a digital panoramic scanning with advanced pathology image analysis system (Wisleap-WS-10, China).

Immunofluorescence (IF) staining of CD31 and α-SMA was used to evaluate angiogenesis in wound areas. Followed the similar procedure mentioned in Sect. 2.2.3, rabbit anit-CD31 primary antibody (1:100, Servicebio, China) and mouse anti-α-SMA primary antibody (1:200, Servicebio, China), Cy3-labeled goat anti-rabbit IgG (1:300, Servicebio, China), and Alexa Fluor 488-labeled goat anti-mouse IgG (1:400, Servicebio, China) were used. The sections were imaged under a panoramic 250/MIDI scanner (3DHISTech, Hungary) with CaseView2.0 software. Mean fluorescence intensity (MFI) was measured by using ImageJ software.

2.13 Statistical analysis

All data were presented as mean ± standard deviation (SD) from at least three samples. Statistical significance was assessed using Student's t-test for paired samples and one-way ANOVA for multiple group comparisons via GraphPad Prism 8.0 software. A p-value of less than 0.05 was considered statistically significant.

3 Results and discussion

3.1 Identification of polarized macrophages

In this study, the naïve M0 macrophages (M0 group) were supposed to be polarized towards M1 phenotype (M1 group) under the stimulation of LPS and INF-γ, and M2 phenotype (M2 group) under the stimulation of IL-4. Here, the polarization status of M0, M1, M2 groups were further identified.

When macrophages are subjected to corresponding stimuli, such as bacterial infection or LPS stimulation, they release sufficient nitric oxide (NO) to inhibit pathogen growth and replication. Thus, NO is an important pro-inflammatory factor, which is highly expressed in the M1 polarized macrophages [29]. As shown in Fig. 1a, on day 1 and 2, M1 group indeed had a significantly higher NO level than M0 and M2 groups ($p < 0.001$). Moreover, M1 macrophages often exhibit a strong inflammatory response by producing pro-inflammatory cytokines (e.g., TNF-α, IL-1β, IL-6, CCL2) and highly expressing iNOS. While, M2 macrophages often show anti-inflammatory and tissue repair functions by releasing anti-inflammatory cytokines (e.g., IL-10), and highly expressing ARG and specific surface markers (e.g., CD206) [30, 31]. Thus, these factors were used as specific phenotypic markers to identify the macrophage polarization by using qRT-PCR and IF staining assays. As shown in Fig. 1b, M0 group always exhibited the lowest expression of either M1 or M2 phenotypic marker genes. Compared to M1 one, M2 group significantly up-regulated the expression of M2 phenotypic marker genes (*Cd206* and *Arg*), but down-regulated the gene expression of M1 phenotypic marker (*iNos*) and inflammatory cytokines (*Tnfα*, *Il1*, *Il6*) ($p < 0.001$). As shown in Fig. 1c–f, it was found that M1 group had the highest M1 marker (iNOS) expression but the lowest M2 marker (CD206) expression, while, M2 group had the highest CD206 expression and CD206/iNOS ratio but the lowest iNOS expression. These results demonstrated that under the different stimuli, the naive M0 macrophages were successfully polarized into M1 and M2 phenotypes.

3.2 Characterization of isolated MΦ-Exos

After differential ultra-centrifugation, MΦ-Exos derived from M0, M1, and M2 phenotypes were isolated, and named as M0-Exos, M1-Exos, and M2-Exos, respectively. Then, the purified MΦ-Exos were further identified by using TEM and Nanoflow cytometry. TEM images found that all isolated vesicles exhibited typical spherical shape with double layered membranes (Fig. 2a), and the comparable sizes as 102.53 ± 9.78 nm, 99.08 ± 15.14 nm, and 98.94 ± 12.13 nm, respectivley (Fig. 2b). Moreover, Nanoflow cytometric analysis (Fig. 2c) showed that

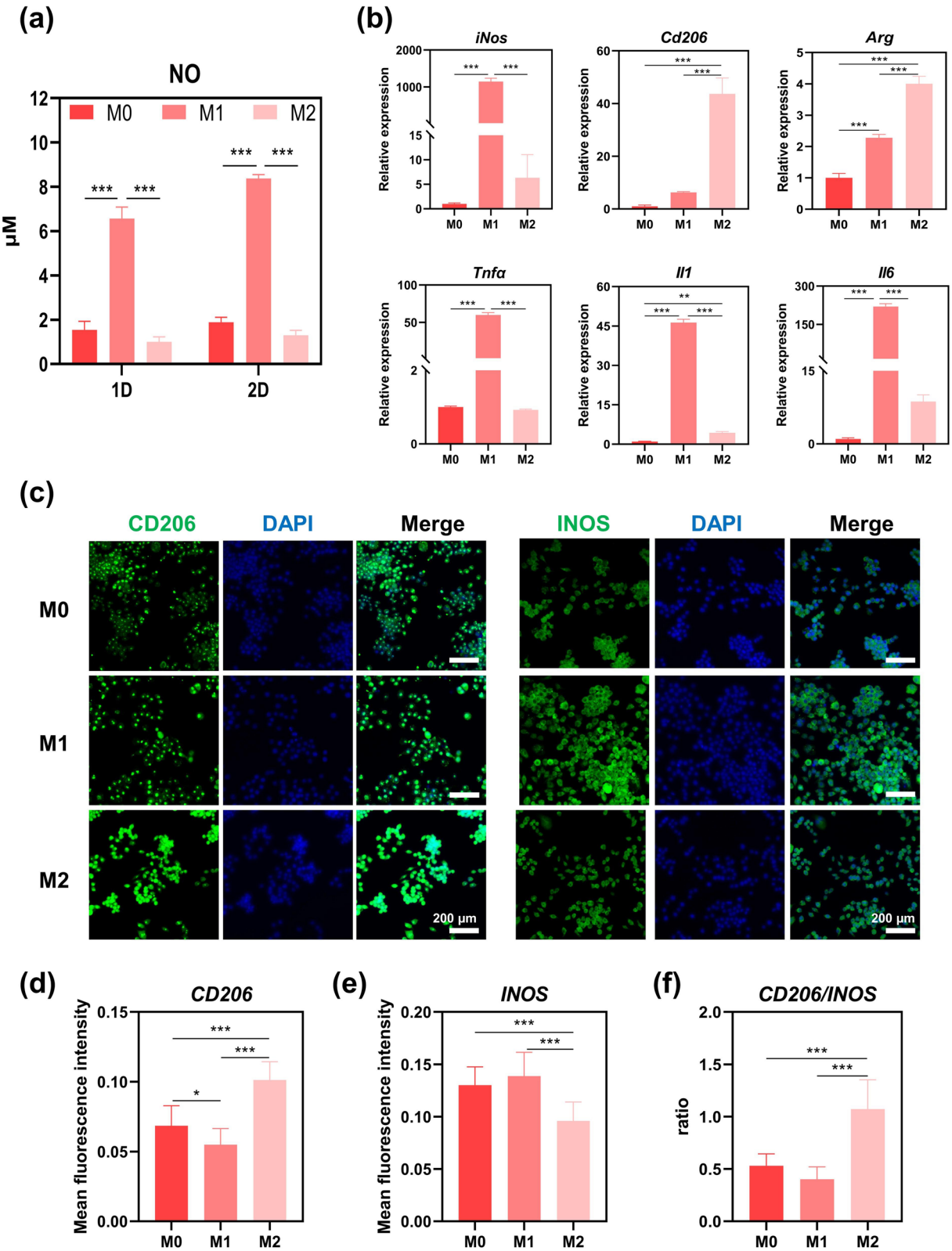

Fig. 1 Identification of polarized macrophages. **a** NO levels in M0, M1, and M2 macrophage on day 1 and 2 (n = 3). **b** The gene expression of M1 markers (*iNos*), M2 markers (*Cd206* and *Arg*), and inflammatory cytokines (*Tnfa*, *Il1*, and *Il6*) in M0, M1, and M2 macrophage on day 2 (n = 3). **c** Immunofluorescence (IF) staining for M1 phenotypic marker (iNOS) and M2 phenotypic marker (CD206). Green: iNOS or CD206; blue: nuclei. The MFI of **d** CD206 and **e** iNOS on day 2, and **f** the ratio of CD206/iNOS (n = 14). * refers to $p < 0.05$, ** refers to $p < 0.01$, *** refers to $p < 0.001$

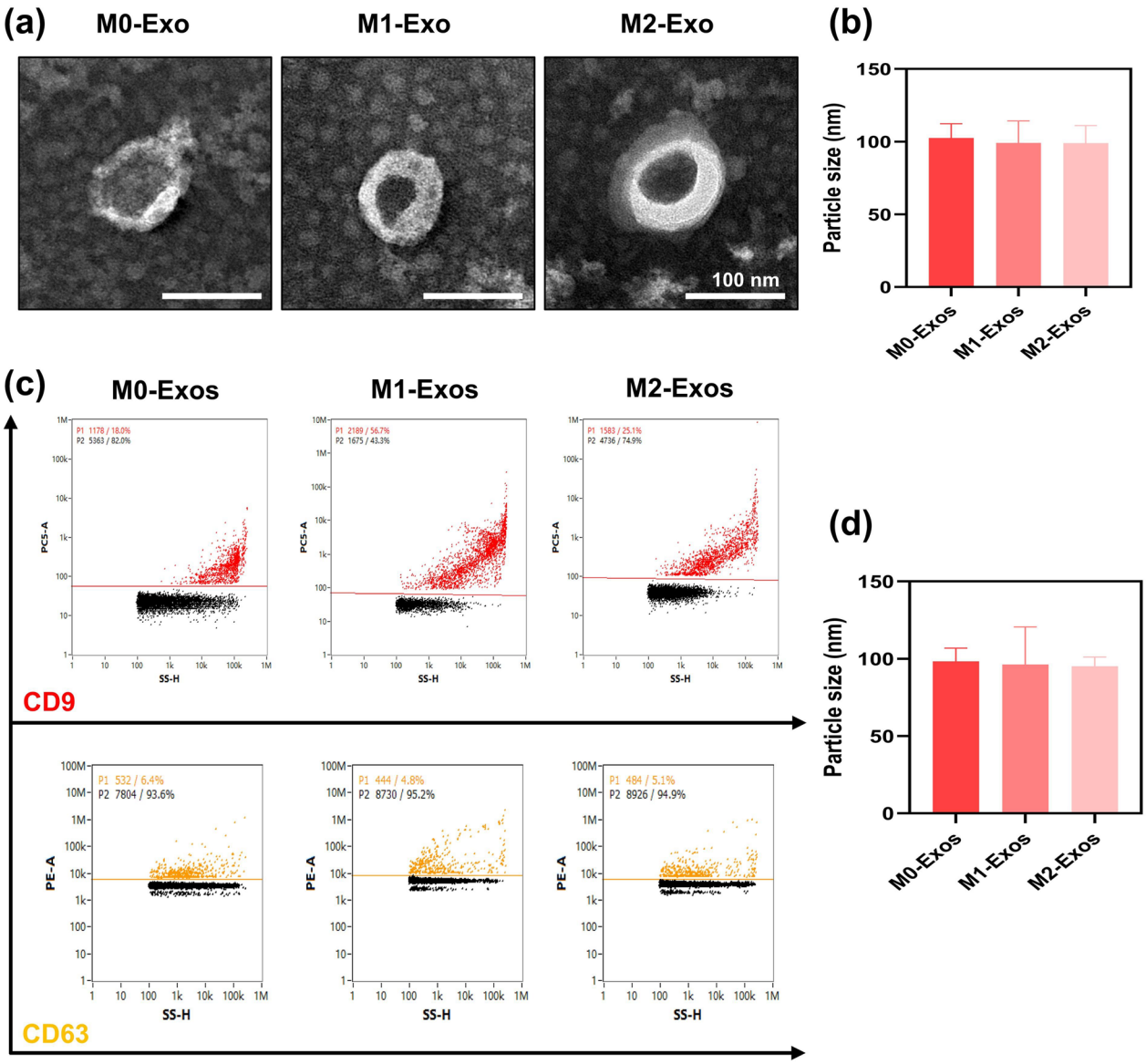

Fig. 2 Characterization of isolated MΦ-Exos. **a** TEM images of the morphology of MΦ-Exos. **b** The average sizes of MΦ-Exos were measured based on TEM images (n = 8). **c** The expression of exosomal markers (i.e., CD9 and CD63) and **d** average sizes of MΦ-Exos were characterized by Nanoflow cytometric analysis (n = 4)

all isolated vesicles positively expressed the exosomal markers (CD9 and CD63), and had the comparable sizes as 98.34 ± 8.51 nm, 96.37 ± 24.22 nm and 95.17 ± 5.96 nm, respectivley (Fig. 2d). It is well known that exosomes refer to a type of extracellular vesicles (EVs), which exhibit membrane-bound sphere or cup-shaped morphology with a size ranging from 30 to 200 nm and express exosomal surface markers [32]. Therefore, in according to the International Society for Extracellular Vesicles (ISEV) position paper, our results suggested that these isolated vesicles displayed the characteristic features of exosomes.

3.3 Effects of MΦ-Exos on angiogenic differentiation of HUVECs in vitro

Images showed that after co-cultured for 12 h, the overlap of intensely perinuclear green fluorescence (PKH67-labeled MΦ-Exos) and the red fluorescence (cytoskeleton) was clearly seen, indicating that M0-Exos, M1-Exos, and M2-Exos could be successfully uptaken by HUVECs (Fig. 3a). The endocytosis of MΦ-Exos was also semi-quantitatively evaluated, suggesting that the MFI of all groups was comparable (Fig. 3b).

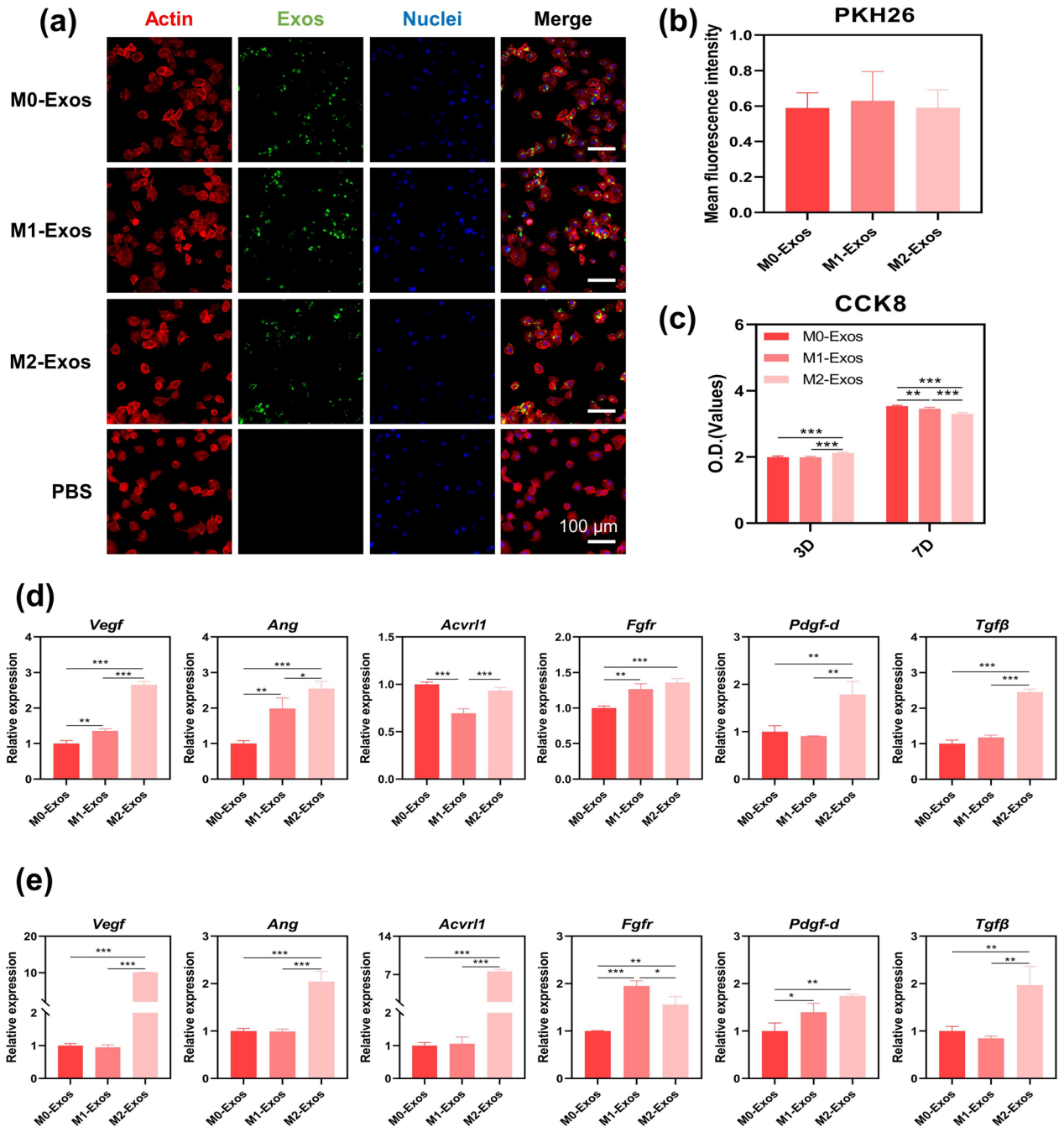

Fig. 3 **a** The differential engulfment of MΦ-Exos in HUVECs was characterized. Red: cytoskeleton; Green: PKH67-labeled MΦ-Exos; Blue: DAPI-labeled cell nuclei. **b** The mean fluorescence intensity (MFI) of M0-Exos, M1-Exos, and M2-Exos (n = 6). **c** CCK-8 results of HUVECs treated with M0-Exos, M1-Exos, or M2-Exos on day 3 and 7 (n = 6). The expression of angiogenesis-related genes in HUVECs treated by MΦ-Exos for **d** 3 Days and **e** 7 Days, including Vegf, Ang, Acvrl1, Fgfr, Pdgf-d, and Tgfβ was characterized by qRT-PCR (n = 3). * refers to $p < 0.05$, ** refers to $p < 0.01$, *** refers to $p < 0.001$

The effects of MΦ-Exos on the proliferation of HUVECs were assessed by CCK-8 assay. As shown in Fig. 3c, on day 3, compared with M0-Exos and M1-Exos, M2-Exos significantly promoted the proliferation of HUVECs ($p < 0.001$). On day 7, M0-Exos group exhibited the highest proliferation rate, followed by M1-Exos group, whereas M2-Exos group demonstrated the lowest rate of proliferation. It was consistent with previous

studies, suggesting that Exos derived from anti-inflammatory M2 macrophages (M2-Exos) could promote the early cell proliferation [33].

To investigate the effects of MΦ-Exos on angiogenic differentiation of HUVECs, qRT-PCR assay was performed to measure the angiogenesis-related genes, such as *Vegf*, *Ang*, *Acvrl1*, *Fgfr*, *Pdgf-d*, and *Tgfβ*. qRT-PCR results (Fig. 3d–e) showed the expression of *Vegf* and *Ang* genes showed the similar trends with the expression levels from high to low as M2-Exos ≥ M1-Exos ≥ M0-Exos ($p < 0.05$). For *Acvrl1* gene, its lowest expression was found in M1-Exos on day 3 ($p < 0.001$), while its highest expression was found in M2-Exos on day 7 ($p < 0.001$). For *Fgfr* gene, its lowest expression was always found in M0-Exos ($p < 0.01$), and its highest expression was found in M1-Exos on day 7 ($p < 0.05$). For *Pdgf-d* and *Tgfβ* gene, its highest expression was always found in M2-Exos ($p < 0.05$). Literature has demonstrated that these factors play a critical role in the angiogenesis process. For instance, vascular endothelial growth factor (VEGF) is also known as angiopoietin, which is of great importance to enhance the proliferation and migration of endothelial cells, thereby inducing the formation and growth of new blood vessels [34]. Angiotensin (Ang) shows the ability to promote the survival, proliferation, and differentiation of endothelial cells, and also recruit and activate adventitial cells such as smooth muscle cells and pericytes, thereby accelerating the formation of new blood vessels and maintaining vascular stability [35]. Activin A receptor type II-like 1 (Acvrl1), also known as ALK1, is an endothelial-specific receptor, which can bind to ligands like bone morphogenetic protein (BMP)-9/10 and Activin to activate downstream TGF-β signaling pathway, thereby regulating vascular development and stability, as well as endothelial cell function [36]. Fibroblast growth factor receptor (FGFR) can activate downstream signaling pathways by binding to FGF to regulate endothelial cell proliferation, migration, and lumen formation, thereby supporting the formation and growth of new blood vessels [37]. Platelet-derived growth factor (PDGF-D) is mainly associated with initiating the process of angiogenesis by promoting cell proliferation, migration, and survival, especially under pathological conditions [38]. Therefore, qRT-PCR results indicated that M2-Exos exhibited significantly enhanced pro-angiogenic potential compared to M0-Exos and M1-Exos.

Moreover, the expression of angiogenic protein (VEGF) in MΦ-Exos-treated HUVECs was measured by IF on day 3 and 7. As shown in Fig. 4a–b, on day 3, M2-Exos group had the highest MFI of VEGF stain, followed by M1-Exos group, and M0-Exos group had the lowest MFI ($p < 0.05$). On day 7, M2-Exos group had the highest MFI of VEGF stain ($p < 0.001$), and the MFI in M0-Exos and M1-Exos were comparable ($p > 0.05$). The effects of MΦ-Exos on the migration of HUVECs were also analyzed by the scratch wound assay. As shown in Fig. 4c–d, there was no significant difference in the migration rate of HUVECs treated with M0-Exos, M1-Exos, or M2-Exos for 12 h, while the migration rate of HUVECs treated with M0-Exos was significantly lower than that treated with M1-Exos and M2-Exos for 24 h. The tube forming assay was also performed to investigate the effect of MΦ-Exos on angiogenesis by measuring the number and length of the capillary-like structures in matrigel. As shown in Fig. 4e–f, compared with M0-Exos and M1-Exos, M2-Exos significantly promoted the vasculature development. Our findings suggested that MΦ-Exos derived from differentially polarized macrophages could impact the angiogenic differentiation of HUVECs. M2-Exos exhibited the superior pro-angiogenic ability in vitro, as evidenced by the higher expression of angiogenic specific genes and proteins, the faster cell migration, and the accelerated tube formation.

3.4 The differentially expressed miRNAs (DEMs) in MΦ-Exos

Exosomes are crucial paracrine mediators derived from their parent cells, which play a pivotal role in intercellular communication by encapsulating and transporting a variety of biologically active molecules such as proteins, nucleic acids, and lipids [14, 15, 21, 39, 40]. Among them, microRNAs (miRNAs), as small non-coding RNAs, are of particular significance due to their potent role in post-transcriptional regulation of gene expression through inhibiting the translation of target mRNA, thereby modulating a wide range of biological processes in the recipient cells [41]. In this study, to investigate the underlying mechanism of the regulation of MΦ-Exos on angiogenic

(See figure on next page.)

Fig. 4 The effects MΦ-Exos on angiogenic protein expression and migration of HUVECs. **a** The expression of VEGF in MΦ-Exos-treated HUVECs was characterized by immunofluorescence staining (IF). Red: VEGF; Blue: DAPI-labeled cell nuclei. **b** The MFI of VEGF staining (n = 15). **c** Optical micrographs of HUVEC migration. **d** The migration rate of HUVECs treated with MΦ-Exos for 12 and 24h (n = 10). **e** Optical micrographs of tube formation. **f** The quantitative data of tube formation includes the number of nodes, junctions, meshes, segments, master junctions, and master segments, as well as total length and branching length (n = 10). * refers to $p < 0.05$, ** refers to $p < 0.01$, *** refers to $p < 0.001$

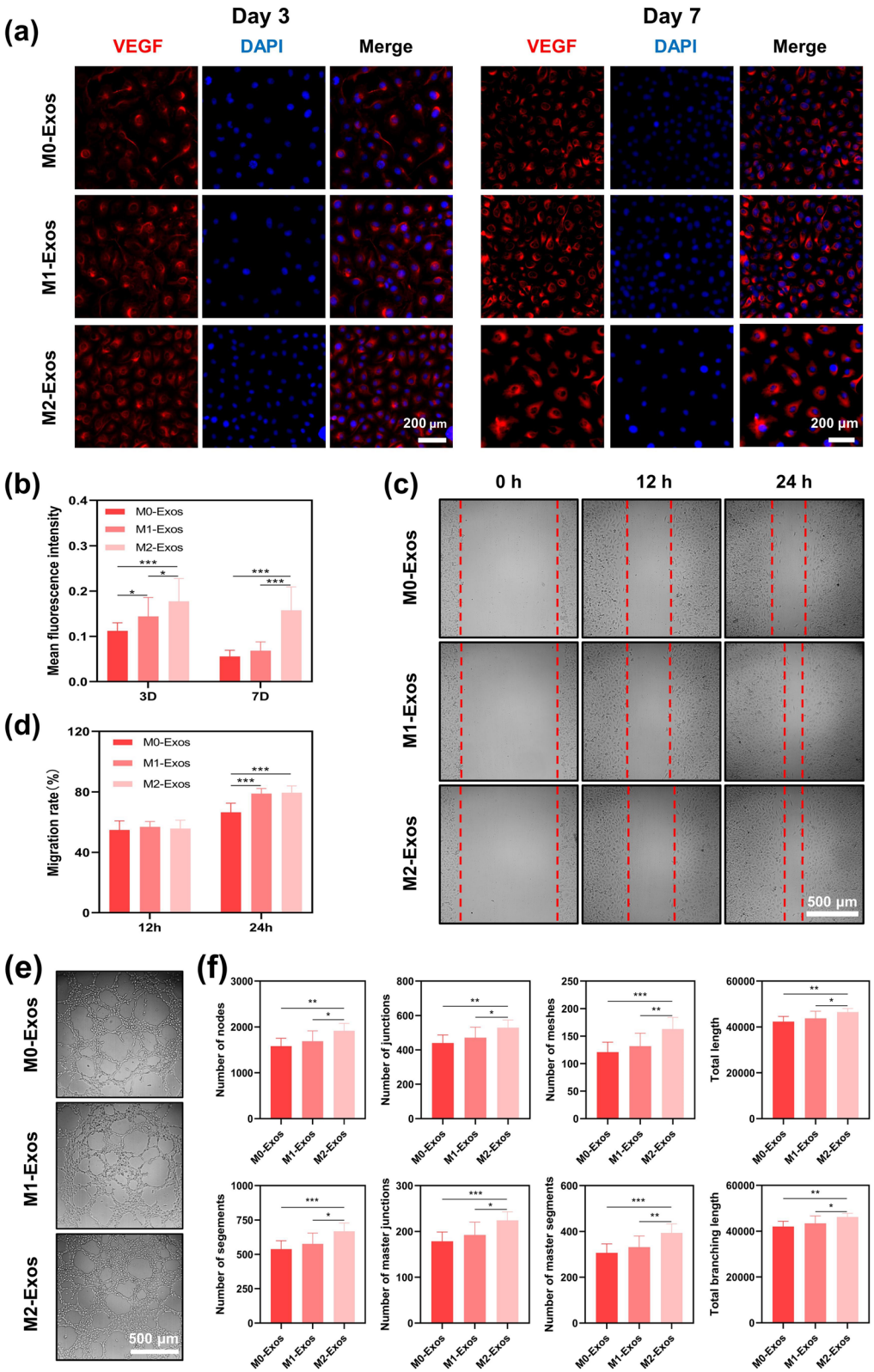

Fig. 4 (See legend on previous page.)

differentiation of HUVECs, the miRNAs associated with angiogenesis in MΦ-Exos cargos were analyzed by qRT-PCR assay. As shown in Fig. 5a, a distinct miRNA expression profile was observed among M0-Exos, M1-Exos, and M2-Exos. Notably, compared to M2-Exos, M1-Exos significantly up-regulated the expression of miRNAs that have been documented in the literature as inhibitors of angiogenesis, including miR-19a-3p [42], miR-23a-3p [43], miR-17-5p [44], miR-155-5p [45], miR-125b-5p [46], miR-125a-3p [47], miR-26a-5p [48], miR-146a-5p [49], miR-210-3p [50], miR-145a-5p [51], miR-150-5p [52], miR-107-3p [53] and miR-27b-3p [54], but down-regulated the expression of miRNAs known to facilitate angiogenic processes, including miR-214-3p [55] and miR-21a-5p [56]. As shown in Fig. 5b, intersection analysis of the three databases using Venny 2.1.0 identified a total of 387 target genes.

KEGG and GO analyses were further used to identify the significantly enriched pathways and the correlative terms, which were influenced by these 15 miRNAs in three MΦ-Exos. KEGG pathway analysis (Fig. 5c) showed that the target genes of these miRNAs were mainly involved in signaling pathways related to angiogenesis, including ErbB [57], HIF-1 [58], FoxO [59], Ras [60], JAK-STAT [61], TGF-beta [62] signaling pathways. Moreover, Go analysis (Fig. 5d) demonstrated that the top ten biological process (BP) mainly participated in regulation of transcription from RNA polymerase II promoter, regulation of transcription, signal transduction, protein phosphorylation, cell differentiation, and so on. The top ten cellular component (CC) mainly affected cytosol, nucleus, cytoplasm, chromatin, Golgi apparatus, and so on. The top molecular function (MF) was identified as protein binding, ATP binding, metal ion binding, protein serine/threonine/tyrosine kinase activity, transcription factor activity, and so on.

Moreover, based on the results of PPI (Fig. 5e) and hub gene analyses (Fig. 5f), the top ten hub genes of differentially expressed miRNAs (DEMs) consisted of *Stat3, Tp53, Bcl2, Smad4, Cdkn1a, Smad3, Smad2, Pik3ca, Foxo1*, and *Igf1r*. Among them, the expression of the main hub genes closely related to angiogenesis in HUVECs such as *Stat3*, *Smad2*, *Smad3*, and *Smad4* were further validated by qRT-PCR (Fig. 5g). It suggested that compared to M0-Exos and M2-Exos, the treatment of M1-Exos indeed significantly down-regulated the gene expression of *Stat3*, *Smad2*, and *Smad4* ($p < 0.05$), but had little effect on *Smad3* expression ($p > 0.05$).

Our findings demonstrated that the differential angiogenic capabilities of exosomes derived from macrophages with varied polarization status might be attributed to the distinct miRNA profiles in MΦ-Exo cargos. M1-Exos were enriched with miRNAs, which could attenuate the target gene expression and inhibit signaling pathways related to angiogenesis (e.g., JAK-STAT and TGF-beta), thereby down-regulating key angiogenic gene expression in HUVECs, and reducing their migration and tubulogenic activities. Conversely, M2-Exos exhibited the opposite effect to promote angiogenesis.

3.5 Characterization of MΦ-Exos-loaded GelMA hydrogels

The colorless mixed solution with MΦ-Exos and GelMA solution rapidly underwent a sol-to-gel transition after exposure to UV light (Fig. 6a). GelMA hydrogels loaded with distinct MΦ-Exos derived from differentially polarized macrophages were prepared for in vivo wound healing, named as Gel, Gel/M0-Exos, Gel/M1-Exos, and Gel/M2-Exos, respectively. As shown in Fig. 6b, the rheological analysis indicated that both the storage modulus (G') and loss modulus (G") of the GelMA hydrogels displayed considerable stability as the angular frequency increased. In addition, the incorporation of exosomes into the GelMA hydrogels did not lead to significant alterations in the values of G' and G". It was consistent with previous studies[27], suggesting that the exosome addition had little impact on the rheological properties of GelMA hydrogels. As shown in Fig. 6c, SEM images suggested that individual exosomes were dispersed in the GelMA hydrogels and the addition of exosomes did not change the macro-porous structure of GelMA hydrogels. Moreover, as shown in Fig. 6d, CLSM images found that all of Dil-labeled MΦ-Exos were evenly distributed in GelMA hydrogels. Furthermore, all MΦ-Exos-loaded GelMA hydrogels exhibited a consistent and slow exosome release up to 9 days (Fig. 6e), which aligned with the time of angiogenesis[63]. These findings suggested that GelMA hydrogel can be used as a sustained-release drug delivery system for exosomes, offering a therapeutic potential for blood circulation reconstruction.

3.6 Effects of MΦ-Exos on wound healing in vivo

MΦ-Exos-loaded GelMA hydrogels were further used for the repair of full-thickness cutaneous wounds in mice (Fig. 6f), following the timeline of animal experiment as shown in Fig. 7a. After surgery, the gross observation of wound closure in the backs of mice was recorded up to 14 days (Fig. 7b). At each time point, we also measured the wound area in each group (Fig. 7c). It was found that the wound sizes of all groups were remarkably reduced with times. Compared to the others, Gel/M2-Exos hydrogel had the faster healing rates during the whole experiment period, and finally the almost complete closure were observed in Gel/M2-Exos group on day 14. However, Gel/M1-Exos notably slowed down the wound healing on day 7, 10 and 14. It suggested that Gel/M2-Exos group had the most efficient wound healing, followed by

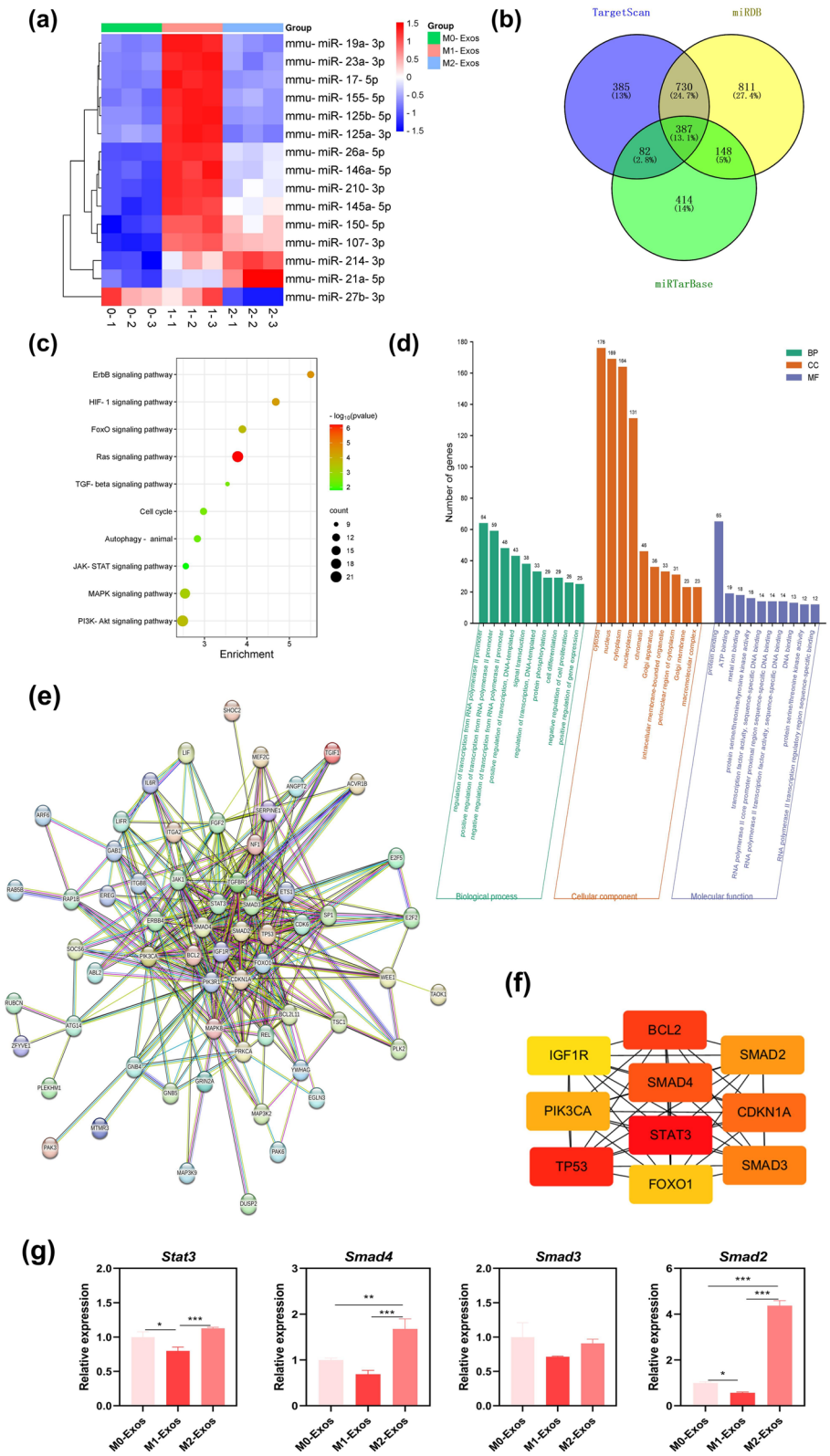

Fig. 5 Bioinformatics analyses of miRNAs with significant differences. **a** Relative expression of miRNAs in M0-Exos, M1-Exos, M2-Exos by qRT-PCR. **b** Venn diagram for screening overlapping target genes across three databases. **c** KEGG analysis of the predicted signaling pathway of target genes. **d** GO analysis of the top ten terms in each category. **e** PPI network of target genes. **f** The top ten hub genes calculated by cytoscape. **g** The expression of angiogenesis-related hub genes in HUVECs (n = 3). * refers to $p < 0.05$, ** refers to $p < 0.01$, *** refers to $p < 0.001$

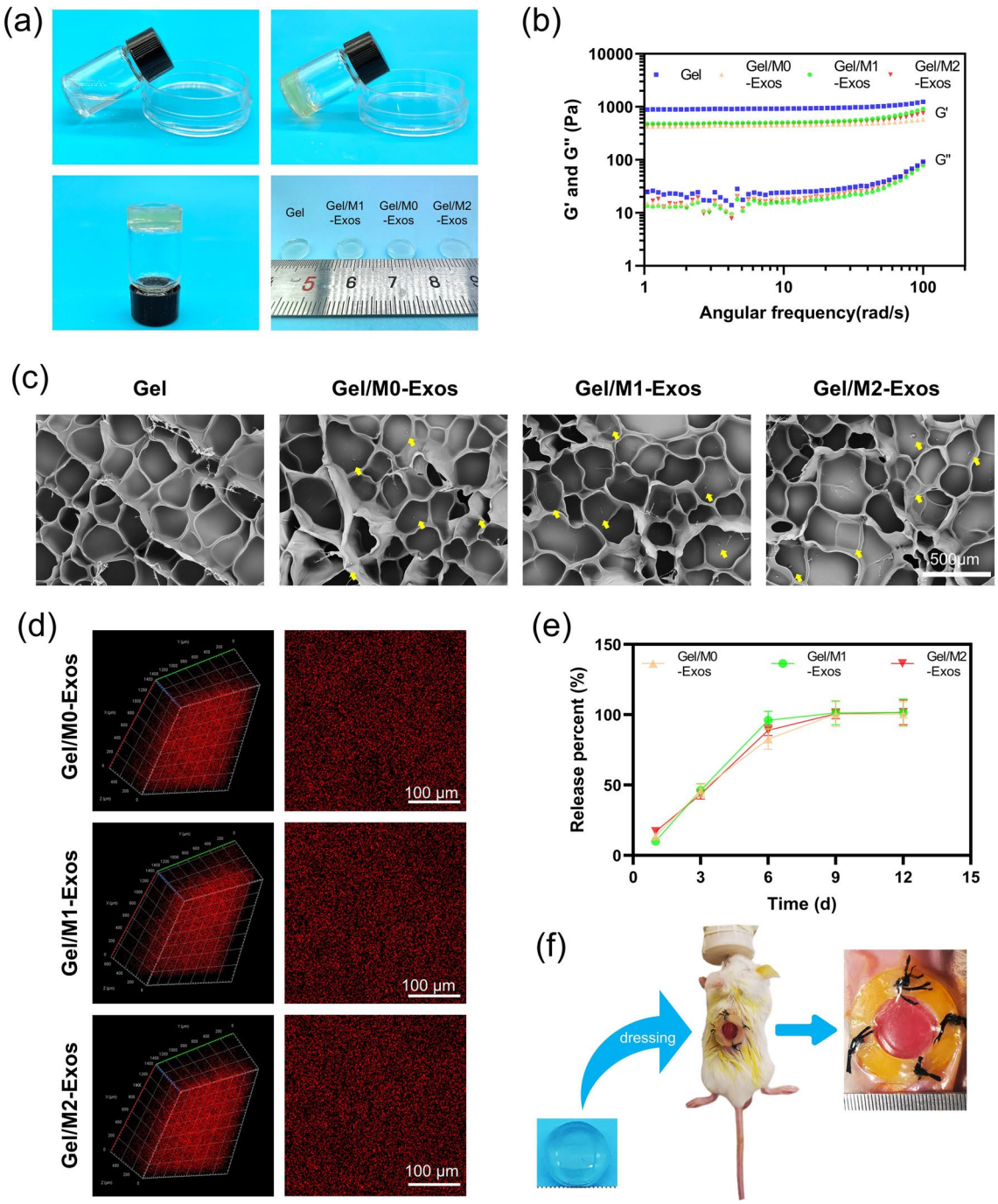

Fig. 6 Characterization of MΦ-Exos-loaded GelMA hydrogels. **a** Optical photos show the sol–gel transition of GelMA hydrogel. **b** Rheological curves and **c** SEM images of GelMA hydrogels (Gel) and exosome-loaded GelMA hydrogels (i.e., Gel/M0-Exos, Gel/M1-Exos, Gel/M2-Exos). Yellow arrows: exosomes. **d** CLSM images showed the even distribution of Dil-labeled MΦ-Exos in GelMA hydrogels. **e** The release of exosomes from three MΦ-Exos-loaded GelMA hydrogels up to 12 days (n = 3). **f** Schematic representation of animal experiment

Gel/M0-Exos group, while Gel/M1-Exos group had the least one.

HE staining was used to assess the wound healing of MΦ-Exos-loaded GelMa hydrogel. As shown in Fig. 8a, abundant granulation tissue was formed in the wound site on day 7, and a remarkable reduction in the wound length was seen on day 14. The length of wound area was calculated and shown in Fig. 8b–c,

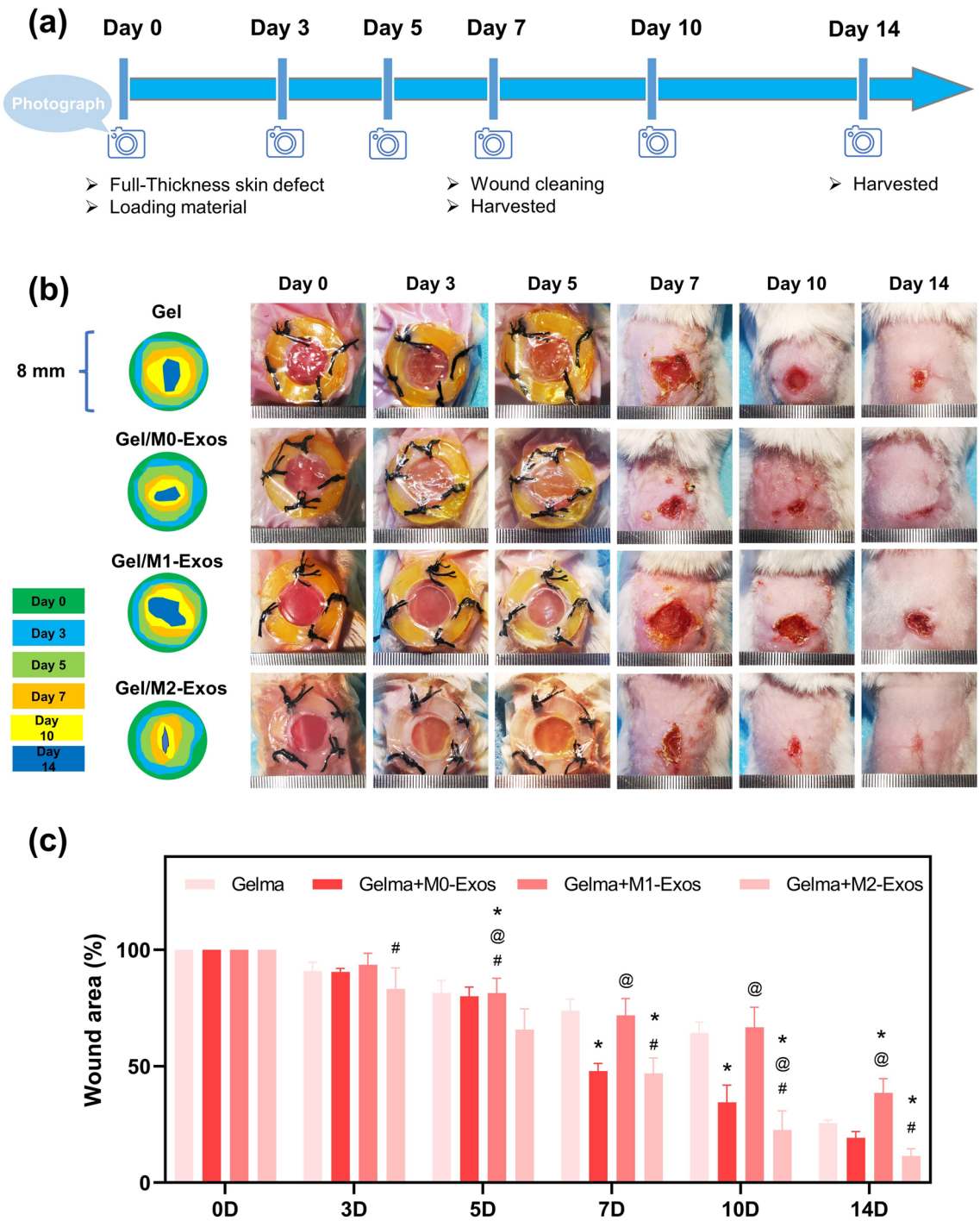

Fig. 7 Wound healing observation in animal experiments. **a** Timeline of animal experiments. **b** Photographs of the Gelma, Gel/M0-Exos, Gel/M1-Exos, and Gel/M2-Exos treated wounds on day 0, 3, 5, 7, 10, and 14. **c** Quantitative analysis for the percentage of wound area (n = 4). *: $p < 0.05$ versus Gelma, @: $p < 0.05$ versus Gel/M0-Exos, #: $p < 0.05$ versus Gel/M1-Exos

finding that Gel/M2-Exos group had the shortest wound length, followed by Gel/M0-Exos, while Gel/M1-Exos and Gel had the longest one on day 7 and 14. High magnification images of HE staining showed that compared to the other groups, complete epithelialization with abundant skin appendages such as hair follicles were only observed in Gel/M2-Exos group on day

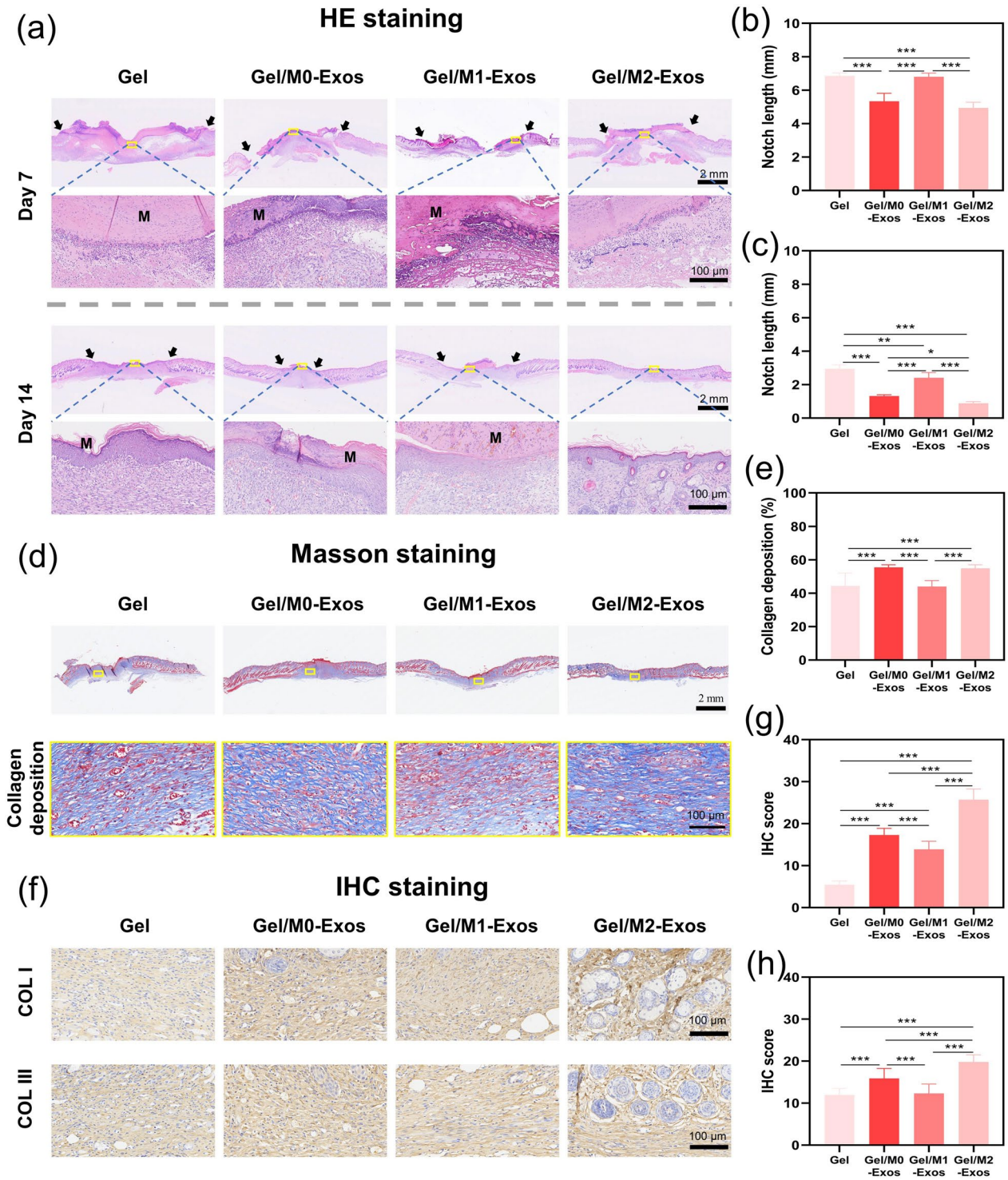

Fig. 8 Representative images of the wound sections stained with **a** Hematoxylin and Eosin (H&E) and quantitative analysis of wound length (n = 4) on **b** day 7 and **c** day 14. M: materials; black arrows: location of wound defect. **d** Images of Masson's trichrome staining and **e** semi-quantitative analysis of collagen deposition on day 14 (n = 8). **f** Images of immumohistochemical (IHC) staining and semi-quantitative analysis (n = 8) for the expression of **g** COL-I and **h** COL-III on day 14. * refers to $p < 0.05$, ** refers to $p < 0.01$, *** refers to $p < 0.001$

14, indicating that almost complete skin repair might be achieved by Gel/M2-Exos treatment.

Collagen deposition and remodeling play an important role in wound healing process, as collagen is a major component of skin tissue to improve the tensile strength of skin [64]. In this study, Masson's trichrome staining was used to evaluate the deposition of collagen in wound sites. It was found that Gel/M2-Exos group exhibited abundant and well-organized collagen fibers, followed by Gel/M0-Exos group, while Gel/M1-Exos and Gel groups showed fewer and loosely packed collagen fibers (Fig. 8d). The semi-quantitative analysis results suggested that the percentage of collagen deposition was from high to low as Gel/M2-Exos ≈ Gel/M0-Exos > Gel/M1-Exos ≈ Gel (Fig. 8e). Moreover, mature epithelial structure and skin appendages were clearly observed in Gel/M2-Exos group, which was in agreement with HE staining results.

The composition of newly-formed skin tissue was further analyzed by IHC staining (Fig. 8f). In the initial phase of wound healing, a rapid accumulation of Type III collagen (COL-III) at the injury site occurs, forming a provisional matrix, which not only stabilizes the wound, but also facilitates the infiltration of cellular components essential for healing [65]. During the remodeling phase, COL-III is gradually replaced by type I collagen (COL-I), which is predominant in dermal extracellular matrix (ECM) of mature skin for restoring structural integrity and mechanical strength of the skin [66, 67]. Our results found that Gel/M2-Exos group had the highest expression of COL-I (Fig. 8g) and COL-III (Fig. 8h), followed by Gel/M0-Exos group, and Gel/M1-Exos and Gel groups had the lowest one.

These findings suggested that GelMA hydrogel loaded with MΦ2-derived Exos (Gel/M2-Exos) could promote the healing of full-thickness wounds, as evidenced by accelerated wound closure, complete epithelialization with hair follicles, and enhanced collagen deposition.

3.7 Effects of MΦ-Exos on angiogenesis in vivo

Angiogenesis is a biological process responsible for the formation of new blood vessels, such as endothelial cell proliferation, migration, and tubular structure formation. Crucially, angiogenesis plays a pivotal role in determining the outcome of wound healing, as the newly formed vasculature facilitates the transport of oxygen and essential nutrients to the wound site [68]. In this study, the angiogenesis in wound sites was further observed by the gross observation, HE staining, and immunofluorescence (IF) staining. As shown in Fig. 9a, the representative photographs showed the angiogenesis state in wound bed. The number of newly-formed blood vessels nodes in wound beds on day 7 and day 14 was shown in Fig. 9b–c. It was found that Gel/M2-Exos group had the most intense capillary network in the center of wound site on day 7, followed by Gel/M0-Exos group, while Gel/M1-Exos and Gel groups had the least one. Up to day 14, the neovascularization had a dramatic decline in Gel/M0-Exos and Gel/M2-Exos groups, while Gel/M1-Exos group showed a slight increase in blood vessel density. Moreover, the expression of angiogenic genes was also analyzed by in vivo qRT-PCR assay (Fig. 9d–e). On day 7, Gel/M1-Exos group dramatically down-regulated the expression of many angiogenic genes, including *Vegf*, *Ang*, *Acvrl1*, *Fgfr*, *Tgfβ*, and *Pdgf-d* ($p < 0.05$). While, compared to Gel/M0-Exos and Gel/M1-Exo ones, Gel/M2-Exos group showed a significantly higher expression of *Vegf*, *Ang*, and *Acvrl1* genes ($p < 0.05$). On the contrary, on day 14, Gel/M1-Exos group up-regulated the expression of *Vegf*, *Ang*, *Acvrl1*, and *Pdgf-d* genes ($p < 0.001$).

The results of HE staining showed on day 7, the MVD (microvessel density) in wound areas ranged from high to low as Gel/M2-Exos ≈ Gel/M0-Exos > Gel/M1-Exos > Gel (Fig. 10a, b). On day 14, the highest MVD was found in Gel/M1-Exos group, while the other groups were comparable (Fig. 10a, c). Moreover, immunofluorescence (IF) staining of CD31 and α-SMA was further employed to evaluate neovascularization formation and maturity. CD31, also known as platelet/endothelial cell adhesion molecule-1, is a cell surface glycoprotein that plays a crucial role in vascular endothelial cells, and thus CD31 is often used as a typical marker of blood vessel [69]. α-SMA, also known as alpha smooth muscle actin, is not only overexpressed in scar tissue but also serves as a marker for mature vascular smooth muscle cells. Its co-localization with CD31 is indicative of the maturation process within the vascular system[69, 70]. The results of IF staining was basically consistent with HE staining (Additional file 2: Fig. S3a–c). Compared to Gel/M1-Exos, Gel/M2-Exos and Gel/M0-Exos groups showed a significantly higher CD31 and α-SMA expression on day 7 (Additional file 2: Fig. S3a–b), but a lower CD31 and α-SMA expression on day 14 (Additional file 2: Fig. S3c–d). In immunofluorescence colocalization analysis, Pearson's coefficient can be used to characterize the spatial distribution similarity of two fluorescent markers, thus reflecting their degree of co-localization in cells or tissues[71]. The results of Pearson's coefficient for colocalization of α-SMA and CD31 was shown in Fig. 10e–f), Similarly, compared to Gel/M1-Exos, Gel/M2-Exos and Gel/M0-Exos groups showed a significantly higher Pearson's coefficient on day 7 (Fig. 10e), but a lower Pearson's coefficient on day 14 (Fig. 10f). Our results suggested that MΦ-Exos encapsulated into GelMa hydrogels might promote the early angiogenesis in wound bed, in particular the ones derived from M0 and M2 macrophages (M0-Exos and M2-Exos). Compared to M0-Exos and

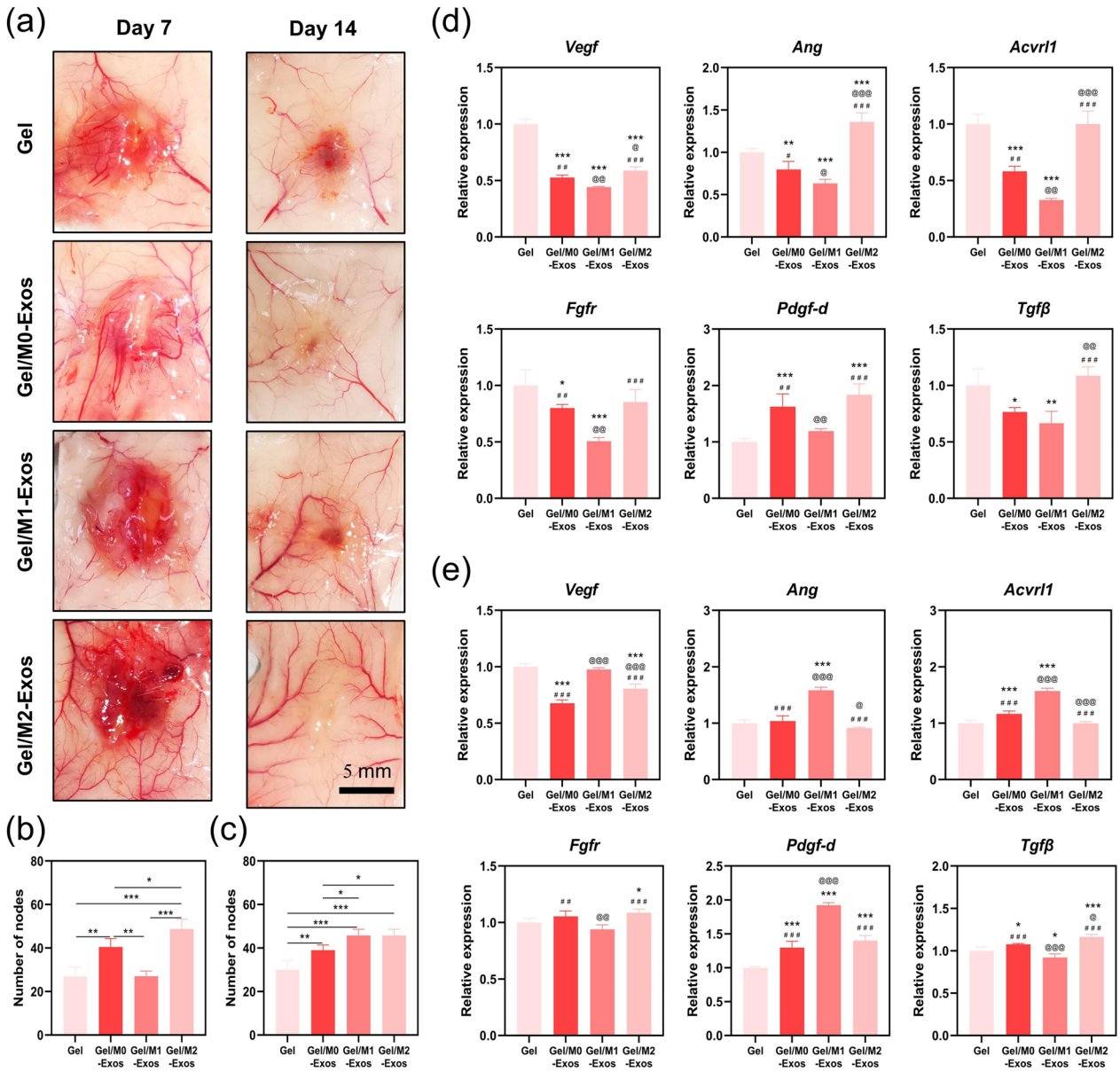

Fig. 9 The effects of MΦ-Exos-loaded GelMA hydrogels on in vivo angiogenesis. **a** Gross observation of newly-formed blood vessels in wound beds on day 7 and day14. The number of newly-formed blood vessels nodes in wound beds on **b** day 7 and **c** day 14 (n = 4). The expression of angiogenesis-related genes in vivo on **d** day 3 and **e** day 7, including Vegf, Ang, Acvrl1, Fgfr, Pdgf-d and Tgfβ (n = 3). * refers to $p < 0.05$ versus Gel, ** refers to $p < 0.01$ versus Gel, *** refers to $p < 0.001$ versus Gel. @ refers to $p < 0.05$ versus Gel/M0-Exos, @@ refers to $p < 0.01$ versus Gel/M0-Exos, @@@ refers to $p < 0.001$ versus Gel/M0-Exos. # refers to $p < 0.05$ versus Gel/M1-Exos, ## refers to $p < 0.01$ versus Gel/M1-Exos, ### refers to $p < 0.001$ versus Gel/M1-Exos

M2-Exos, M1-Exos might delay the angiogenesis process, as the expression of angiogenic genes (e.g., *Vegf*, *Ang*, *Acvrl1*, *Fgfr*, *Pdgf-d*, and *Tgfβ*) and proteins (e.g., CD31 and α-SMA) in M0-Exos and M2-Exos reached the peak on day 7, while their expression in M1-Exos peaked on day 14.

In summary, these findings provided compelling evidence that GelMA hydrogels loaded with exosomes derived from macrophages in different polarization states (MΦ-Exos) significantly influenced angiogenesis, thereby impacting the wound healing process. Compared to M0-Exos and M1-Exos, M2-Exos notably enhanced HUVEC migration and tube formation, and M2Φ-Exos-loaded GelMA hydrogels dramatically accelerated angiogenesis in mouse full-thickness skin wound model, suggesting that M2-Exos exhibited a pronounced

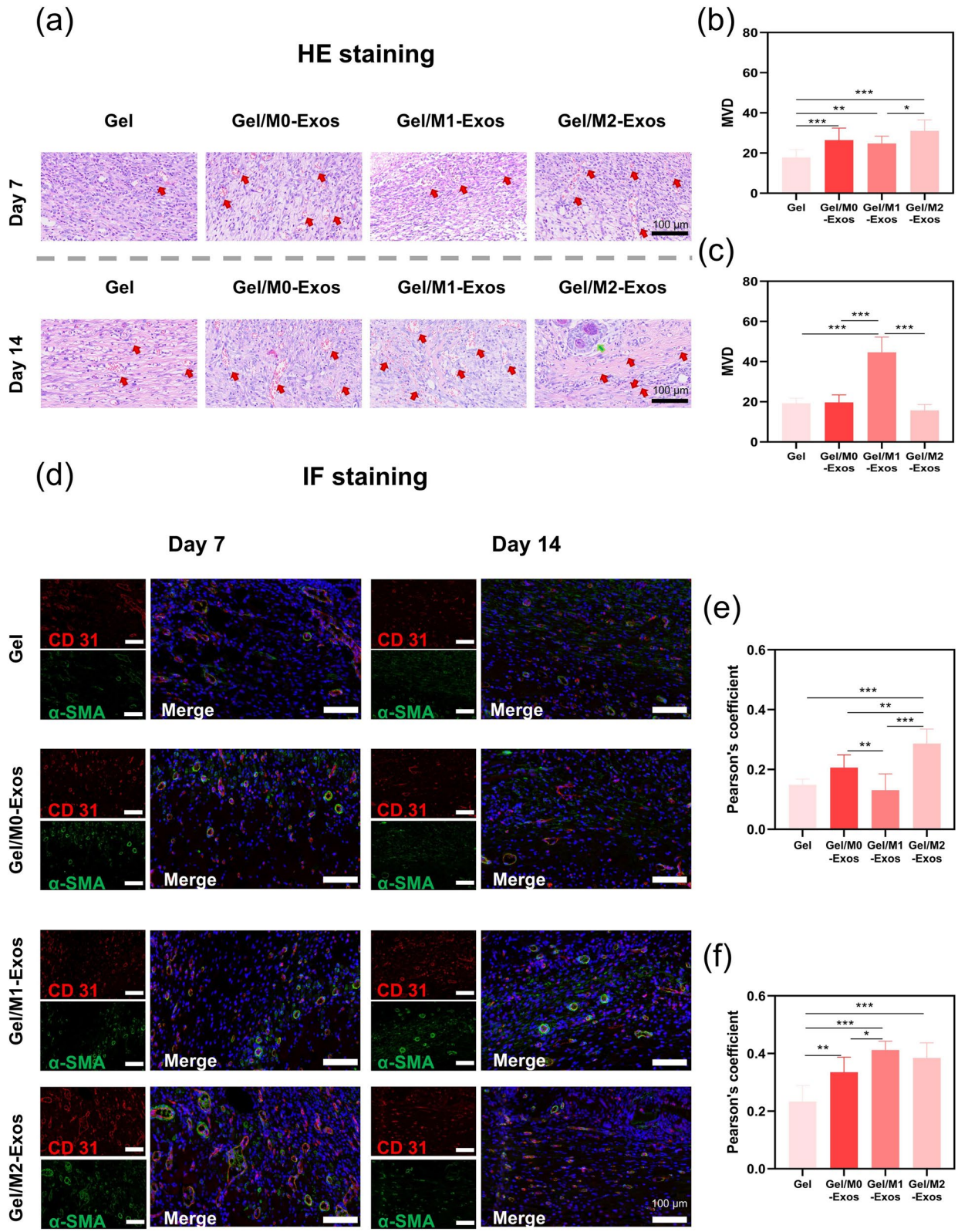

Fig. 10 **a** Representative images of granulation tissue stained with Hematoxylin and Eosin (H&E), and quantitative analysis of MVD (microvessel density) on **b** day 7 and **c** day 14 (n = 8). Red arrow: microvessel; green arrow: new hair follicles. **d** Immunofluorescence (IF) co-staining for CD31 and α-SMA in the granulation tissue. The Pearson's coefficient correlated with the co-localization of CD31 and α-SMA on day 7 **e** and day 14 **f** (n = 8). * refers to $p < 0.05$, ** refers to $p < 0.01$, *** refers to $p < 0.001$

potential to enhance angiogenesis. It highlighted a delicate role of macrophage polarization in tissue repair and regeneration, and aligned with the growing consensus that M2 macrophages play a crucial role in promoting angiogenesis by enhancing HUVEC migration, tubule formation, and aortic ring germination [16, 17, 19, 20]. It might be attributed to the differential miRNA expression profiles within distinct MΦ-Exos, which was investigated by qRT-PCR and bioinformatics analysis that identified the key angiogenesis-associated miRNAs and their target genes, as well as related signaling pathways (e.g., JAK-STAT and TGF-β). Future research may further explore the underlying mechanism of the pro-angiogenic ability of M2Φ-Exos-loaded GelMA hydrogels, in particular focusing on the functions of differentially expressed miRNAs in M2-Exos via a variety of experimental approaches such as luciferase reporter assays, miRNA mimics/inhibitors, and RNA interference (RNAi).

4 Conclusion

Our findings highlight the potential of the exosomes derived from M2-polarized macrophages (M2-Exos) as nano-scaled, cell-free therapeutic agents with potent pro-angiogenic ability. Moreover, these findings suggested that GelMA hydrogel holds promise as a sustained-release drug delivery system suitable for exosomes, and M2Φ-Exos-loaded GelMA hydrogels show multi-functional therapeutic potentials to promote wound healing by accelerating epithelial regeneration, angiogenesis, and collagen deposition.

Abbreviations

MΦ	Macrophages
M0	Naïve macrophages
M1	Pro-inflammatory macrophages
M2	Anti-inflammatory macrophages
MΦ-Exos	Macrophage-derived exosomes
GelMA	Gelatine methacrylate
LPS	Lipopolysaccharides
IFN	Interferon
IL	Interleukin
iNOS	Inducible nitric oxide synthase
TNF	Tumor necrosis factor
ARG	Arginase-1
Exos	Exosomes
HUVECs	Human umbilical vein endothelial cells
NO	Nitric oxide
cDNA	Complementary DNA
PFA	Paraformaldehyde
RT	Room temperature
BSA	Bovine serum albumin
TEM	Transmission electron microscope
DAPI	4′,6-Diamidino-2-phenylindole
CCK-8	Cell Counting Kit-8 assay
IF	Immunofluorescence
KEGG	Kyoto Encyclopedia of Genes and Genome
GO	Gene ontology
PPI	Protein-protein interaction
PTFE	Polytetrafluoroethylene
IHC	Immumohistochemical
Col	Collagen
MFI	Mean fluorescence intensity
VEGF	Vascular endothelial growth factor
Ang	Angiotensin
Acvrl1	Activin A receptor type II-like 1
BMP	Bone morphogenetic protein
FGFR	Fibroblast growth factor receptor
PDGF-D	Platelet-derived growth factor
BP	Biological process
CC	Cellular component
MF	Molecular function

Supplementary Information

The online version contains supplementary material available at https://doi.org/10.1186/s42825-024-00156-8.

Additional file 1. Supplementary Table.

Additional file 2. Supplementary Figures.

Acknowledgements

The authors thank Dr. Guolong Meng and Dr. Jiao Lu (National Engineering Research Center for Biomaterials, Sichuan University) for their help in the characterization of SEM and CLSM.

Author contributions

JJL: Investigation, methodology, data curation, formal analysis, writing original draft; FYC: Data curation, formal analysis; LQT: Investigation, visualization; JJW: Formal analysis; KTL: Investigation, software; QWW: Investigation; BY: Manuscript revision; XNC: Conceptualization, formal analysis, funding acquisition, investigation, project administration, supervision, writing; XDZhu and XDZhang: Project administration, supervision. All authors read and approved the final manuscript.

Funding

This work was sponsored by the National Science Foundation of China (31971283, 31670985), National Key Research and Development Program of China (2017YFB0702602), and Sichuan Science and Technology Innovation Team of China (2019JDTD0008). The authors thank Ms. Jiao Lu and Mr. Guolong Meng at Sichuan University for the assistance in CLSM and SEM measurement.

Availability of data and materials

All the data supporting the fndings of this study are included in this manuscript.

Declarations

Ethics approval and consent to participate

The animal study was approved by the Ethical Committee of Sichuan University (KS2021698). All the animals were purchased from Chengdu dossy experimental animals co., LTD. The animal experiment guidance from the ethical committee and the guide for care and use of laboratory animals of Sichuan University were followed during the whole experiment course.

Consent for publication

Not applicable.

Competing interests

The authors declare that they have no competing interests.

Author details

[1]National Engineering Research Center for Biomaterials, College of Biomedical Engineering, Sichuan University, 29# Wangjiang Road, Chengdu 610064, Sichuan, China. [2]Faculty of Health Sciences, University of Macau, Macau, China.

Received: 11 January 2024 Revised: 6 March 2024 Accepted: 7 March 2024
Published online: 01 May 2024

References

1. Shi S, Wang L, Song C, Yao L, Xiao J. Recent progresses of collagen dressings for chronic skin wound healing. 2023;5(1).
2. Gould J. Superpowered skin. Nature. 2018;563(7732):S84.
3. Heng MCY. Wound healing in adult skin: aiming for perfect regeneration. Int J Dermatol. 2011;50(9):1058.
4. Al SH. Macrophage phenotypes in normal and diabetic wound healing and therapeutic interventions. Cells. 2022;11(15):2430.
5. Lee J-H, Parthiban P, Jin G-Z, Knowles JC, Kim H-W. Materials roles for promoting angiogenesis in tissue regeneration. Prog Mater Sci. 2021;117:100732.
6. Sun X, Altalhi W, Nunes SS. Vascularization strategies of engineered tissues and their application in cardiac regeneration. Adv Drug Deliv Rev. 2016;96:183.
7. Palma MB, Luzzani C, Andrini LB, Riccillo F, Buero G, Pelinski P, et al. Wound healing by allogeneic transplantation of specific subpopulation from human umbilical cord mesenchymal stem cells. Cell Transplant. 1900;2021(30):096368972199377.
8. Krishnasamy K, Limbourg A, Kapanadze T, Gamrekelashvili J, Beger C, Häger C, et al. Blood vessel control of macrophage maturation promotes arteriogenesis in ischemia. Nat Commun. 2017;8(1):952.
9. Gurevich DB, Severn CE, Twomey C, Greenhough A, Cash J, Toye AM, et al. Live imaging of wound angiogenesis reveals macrophage orchestrated vessel sprouting and regression. EMBO J. 2018;37(13):1.
10. Wu G, Mu C, Zhao Q, Lei Y, Cheng R, Nie W, et al. Thylakoid engineered M2 macrophage for sonodynamic effect promoted cell therapy of early atherosclerosis. Nano Res. 2023;
11. Bai B, Gu C, Lu X, Ge X, Yang J, Wang C, et al. Polydopamine functionalized mesoporous silica as ROS-sensitive drug delivery vehicles for periodontitis treatment by modulating macrophage polarization. Nano Res. 2021;14(12):4577.
12. Mantovani A, Sica A, Sozzani S, Allavena P, Vecchi A, Locati M. The chemokine system in diverse forms of macrophage activation and polarization. Trends Immunol. 2004;25(12):677.
13. Han X, Hu J, Zhao W, Lu H, Dai J, He Q. Hexapeptide induces M2 macrophage polarization via the JAK1/STAT6 pathway to promote angiogenesis in bone repair. Exp Cell Res. 2022;413(1): 113064.
14. Zhang Y, Liu Y, Liu H, Tang WH. Exosomes: biogenesis, biologic function and clinical potential. Cell Biosci. 2019;9(1):19.
15. Ma X, Liu B, Fan L, Liu Y, Zhao Y, Ren T, et al. Native and engineered exosomes for inflammatory disease. Nano Res. 2023;16(5):6991.
16 Luo Z, Peng W, Xu Y, Xie Y, Liu Y, Lu H, et al. Exosomal OTULIN from M2 macrophages promotes the recovery of spinal cord injuries via stimulating Wnt/β-catenin pathway-mediated vascular regeneration. Acta Biomater. 2021;136:519.
17. Yang Y, Guo Z, Chen W, Wang X, Cao M, Han X, et al. M2 macrophage-derived exosomes promote angiogenesis and growth of pancreatic ductal adenocarcinoma by targeting E2F2. Mol Ther. 2021;29(3):1226.
18. Liu S, Chen J, Shi J, Zhou W, Wang L, Fang W, et al. M1-like macrophage-derived exosomes suppress angiogenesis and exacerbate cardiac dysfunction in a myocardial infarction microenvironment. Basic Res Cardiol. 2020;115(2):22.
19. Lyu L, Cai Y, Zhang G, Jing Z, Liang J, Zhang R, et al. Exosomes derived from M2 macrophages induce angiogenesis to promote wound healing. Front Mol Biosci. 2022;9(October):1.
20. Liu P, Xiong Y, Chen L, Lin C, Yang Y, Lin Z, et al. Angiogenesis-based diabetic skin reconstruction through multifunctional hydrogel with sustained releasing of M2 Macrophage-derived exosome. Chem Eng J. 2022;431(P1): 132413.
21. Kalluri R, LeBleu VS. The biology, function, and biomedical applications of exosomes. Science(80-). 2020;367(6478):
22. Shan X, Zhang C, Mai C, Hu X, Cheng N, Chen W, et al. The biogenesis, biological functions, and applications of macrophage-derived exosomes. Front Mol Biosci. 2021;8(July):1.
23. Xiang L, Cui W. Biomedical application of photo-crosslinked gelatin hydrogels. J Leather Sci Eng. 2021;3(1).
24. Isik M, Vargel I, Ozgur E, Cam SB, Korkusuz P, Emregul E, et al. Human periodontal ligament stem cells-derived exosomes-loaded hybrid hydrogel enhances the calvarial defect regeneration in middle-age rats. Mater Today Commun. 2023;36(June): 106869.
25. Zhao D, Yu Z, Li Y, Wang Y, Li Q, Han D. GelMA combined with sustained release of HUVECs derived exosomes for promoting cutaneous wound healing and facilitating skin regeneration. J Mol Histol. 2020;51(3):251.
26. Dennis G, Sherman BT, Hosack DA, Yang J, Gao W, Lane HC, et al. DAVID: database for annotation, visualization, and integrated discovery. Genome Biol. 2003;4(9):R60.
27. Sun J, Li G, Wu S, Zou Y, Weng W, Gai T, et al. Engineering preparation and sustained delivery of bone functional exosomes-laden biodegradable hydrogel for in situ bone regeneration. Compos B Eng. 2023;261(March): 110803.
28. Wang C, Wang M, Xu T, Zhang X, Lin C, Gao W, et al. Engineering bioactive self-healing antibacterial exosomes hydrogel for promoting chronic diabetic wound healing and complete skin regeneration. Theranostics. 2019;9(1):65.
29. Drehmer D, Mesquita Luiz JP, Hernandez CAS, Alves-Filho JC, Hussell T, Townsend PA, et al. Nitric oxide favours tumour-promoting inflammation through mitochondria-dependent and -independent actions on macrophages. Redox Biol. 2022;54(May): 102350.
30. Yunna C, Mengru H, Lei W, Weidong C. Macrophage M1/M2 polarization. Eur J Pharmacol. 2020;877(March): 173090.
31. Miao X, Leng X, Zhang Q. The current state of nanoparticle-induced macrophage polarization and reprogramming research. Int J Mol Sci. 2017;18(2):336.
32. Hill AF, Pegtel DM, Lambertz U, Leonardi T, O'Driscoll L, Pluchino S, et al. ISEV position paper: extracellular vesicle RNA analysis and bioinformatics. J Extracell Vesicles. 2013;2(1):1.
33. Deng F, Yan J, Lu J, Luo M, Xia P, Liu S, et al. M2 macrophage-derived exosomal miR-590-3p attenuates DSS-induced mucosal damage and promotes epithelial repair via the LATS1/YAP/ β-catenin signalling axis. J Crohn's Colitis. 2021;15(4):665.
34. Ahmad A, Nawaz MI. Molecular mechanism of VEGF and its role in pathological angiogenesis. J Cell Biochem. 2022;123(12):1938.
35. Xue Y, Cao R, Nilsson D, Chen S, Westergren R, Hedlund E-M, et al. FOXC2 controls Ang-2 expression and modulates angiogenesis, vascular patterning, remodeling, and functions in adipose tissue. Proc Natl Acad Sci. 2008;105(29):10167.
36. Capasso TL, Li B, Volek HJ, Khalid W, Rochon ER, Anbalagan A, et al. BMP10-mediated ALK1 signaling is continuously required for vascular development and maintenance. Angiogenesis. 2020;23(2):203.
37. Ruan R, Li L, Li X, Huang C, Zhang Z, Zhong H, et al. Unleashing the potential of combining FGFR inhibitor and immune checkpoint blockade for FGF/FGFR signaling in tumor microenvironment. Mol Cancer. 2023;22(1):60.
38. Uutela M, Wirzenius M, Paavonen K, Rajantie I, He Y, Karpanen T, et al. PDGF-D induces macrophage recruitment, increased interstitial pressure, and blood vessel maturation during angiogenesis. Blood. 2004;104(10):3198.
39. Xiao Y, Li H, Zhang J, Yang S, Zhang C, Huang Y, et al. Mesenchymal stem cell-derived exosomes: versatile nanomaterials for skin wound treatment. Nano Res. 2023;
40 Johnstone RM, Adam M, Hammond JR, Orr L, Turbide C. Vesicle formation during reticulocyte maturation. Association of plasma membrane activities with released vesicles (exosomes). J Biol Chem. 1987;262(19):9412.
41. Pauley KM, Cha S, Chan EKL. MicroRNA in autoimmunity and autoimmune diseases. J Autoimmun. 2009;32(3–4):189.
42. Liu M, Yang P, Fu D, Gao T, Deng X, Shao M, et al. Allicin protects against myocardial I/R by accelerating angiogenesis via the miR-19a-3p/PI3K/AKT axis. Aging (Albany NY). 2021;13(19):22843.
43. Liu Y, Li Q, Tang D, Li M, Zhao P, Yang W, et al. SNHG17 promotes the proliferation and migration of colorectal adenocarcinoma cells by modulating CXCL12-mediated angiogenesis. Cancer Cell Int. 2020;20(1):566.
44. Zhang Z, Shuai Y, Zhou F, Yin J, Hu J, Guo S, et al. PDLSCs regulate angiogenesis of periodontal ligaments via VEGF transferred by exosomes in periodontitis. Int J Med Sci. 2020;17(5):558.
45. Tong Y, Zhou M-H, Li S-P, Zhao H-M, Zhang Y-R, Chen D, et al. MiR-155-5p attenuates vascular smooth muscle cell oxidative stress and migration via inhibiting BACH1 expression. Biomedicines. 2023;11(6):1679.
46. Ma C, Tang X, Tang Q, Wang S, Zhang J, Lu Y, et al. Curcumol repressed cell proliferation and angiogenesis via SP1/mir-125b-5p/VEGFA axis in non-small cell lung cancer. Front Pharmacol. 2022;13(November):1.

47. Hou P, Li H, Yong H, Chen F, Chu S, Zheng J, et al. PinX1 represses renal cancer angiogenesis via the mir-125a-3p/VEGF signaling pathway. Angiogenesis. 2019;22(4):507.
48. Si Y, Zhang H, Ning T, Bai M, Wang Y, Yang H, et al. miR-26a/b inhibit tumor growth and angiogenesis by targeting the HGF-VEGF axis in gastric carcinoma. Cell Physiol Biochem. 2017;42(4):1670.
49. Pan T, Wu Y, Zhang X, Wang J, Wang X, Gu Q, et al. Lens epithelial cell-derived exosome inhibits angiogenesis in ocular pathological neovascularization through its delivery of <scp>miR</scp> -146a-5p. FASEB J. 2023;37(10):1.
50. Yang Q, Wang P, Du X, Wang W, Zhang T, Chen Y. Direct repression of IGF2 is implicated in the anti-angiogenic function of microRNA-210 in human retinal endothelial cells. Angiogenesis. 2018;21(2):313.
51. Thuringer D, Jego G, Berthenet K, Hammann A, Solary E, Garrido C. Gap junction-mediated transfer of miR-145-5p from microvascular endothelial cells to colon cancer cells inhibits angiogenesis. Oncotarget. 2016;7(19):28160.
52. Chen X, Xu X, Pan B, Zeng K, Xu M, Liu X, et al. Correction for: miR-150-5p suppresses tumor progression by targeting VEGFA in colorectal cancer. Aging (Albany NY). 2021;13(9):13372.
53. Yamakuchi M, Lotterman CD, Bao C, Hruban RH, Karim B, Mendell JT, et al. P53-induced microRNA-107 inhibits HIF-1 and tumor angiogenesis. Proc Natl Acad Sci. 2010;107(14):6334.
54. Dou R, Liu K, Yang C, Zheng J, Shi D, Lin X, et al. EMT-cancer cells-derived exosomal miR-27b-3p promotes circulating tumour cells-mediated metastasis by modulating vascular permeability in colorectal cancer. Clin Transl Med. 2021;11(12).
55. Lan X, Yu R, Xu J, Jiang X. Exosomes from chondrocytes overexpressing miR-214-3p facilitate M2 macrophage polarization and angiogenesis to relieve Legg Calvé-Perthes disease. Cytokine. 2023;168(1519): 156233.
56. Li Y, Chen X, Jin R, Chen L, Dang M, Cao H, et al. Injectable hydrogel with MSNs/microRNA-21-5p delivery enables both immunomodification and enhanced angiogenesis for myocardial infarction therapy in pigs. Sci Adv. 2021;7(9):1.
57. Sini P, Wyder L, Schnell C, O'Reilly T, Littlewood A, Brandt R, et al. The antitumor and antiangiogenic activity of vascular endothelial growth factor receptor inhibition is potentiated by ErbB1 blockade. Clin Cancer Res. 2005;11(12):4521.
58. Mizukami Y, Kohgo Y, Chung DC. Hypoxia inducible factor-1–independent pathways in tumor angiogenesis. Clin Cancer Res. 2007;13(19):5670.
59. Farhan M, Silva M, Xingan X, Huang Y, Zheng W. Role of FOXO transcription factors in cancer metabolism and angiogenesis. Cells. 2020;9(7):1586.
60. Lee S-H, Son MJ, Oh S-H, Rho S-B, Park K, Kim Y-J, et al. Thymosin β10 inhibits angiogenesis and tumor growth by interfering with RAS function. Cancer Res. 2005;65(1):137.
61. Zhang Q, Wang L, Wang S, Cheng H, Xu L, Pei G, et al. Signaling pathways and targeted therapy for myocardial infarction. Signal Transduct Target Ther. 2022;7(1):78.
62. Chiavarina B, Costanza B, Ronca R, Blomme A, Rezzola S, Chiodelli P, et al. Metastatic colorectal cancer cells maintain the TGFβ program and use TGFBI to fuel angiogenesis. Theranostics. 2021;11(4):1626.
63. Wang K, Dong R, Tang J, Li H, Dang J, Zhang Z, et al. Exosomes laden self-healing injectable hydrogel enhances diabetic wound healing via regulating macrophage polarization to accelerate angiogenesis. Chem Eng J. 2022;430(P1): 132664.
64. Jeon EY, Choi B-H, Jung D, Hwang BH, Cha HJ. Natural healing-inspired collagen-targeting surgical protein glue for accelerated scarless skin regeneration. Biomaterials. 2017;134:154.
65. Xue M, Jackson CJ. Extracellular matrix reorganization during wound healing and its impact on abnormal scarring. Adv Wound Care. 2015;4(3):119.
66. Liu R, Dai M, Gong G, Chen M, Cao C, Wang T, et al. The role of extracellular matrix on unfavorable maternal–fetal interface: focusing on the function of collagen in human fertility. J Leather Sci Eng. 2022;4(1).
67. Hooshmand S, Mollazadeh S, Akrami N, Ghanad M, El-Fiqi A, Baino F, et al. Mesoporous silica nanoparticles and mesoporous bioactive glasses for wound management: from skin regeneration to cancer therapy. Materials (Basel). 2021;14(12):3337.
68. Mao C, Xiang Y, Liu X, Cui Z, Yang X, Yeung KWK, et al. Photo-inspired antibacterial activity and wound healing acceleration by hydrogel embedded with Ag/Ag@AgCl/ZnO nanostructures. ACS Nano. 2017;11(9):9010.
69. Liu Y, Zhao F, Song T, Tang M, Tian L, He T, et al. Nanohybrid dual-network chitosan-based hydrogels: synthesis, characterization, quicken infected wound healing by angiogenesis and immune-microenvironment regulation. Carbohydr Polym. 2023;2024(325): 121589.
70. Usuda K, Iwai S, Funasaki A, Sekimura A, Motono N, Ueda Y, et al. expression and prognostic impact of VEGF, CD31 and αSMA in resected primary lung cancers. Anticancer Res. 2018;38(7):4057.
71. Lopez SG, Samwald S, Jones S, Faulkner C. On the pixel selection criterion for the calculation of the Pearson's correlation coefficient in fluorescence microscopy. J Microsc. 2023;2024:1.

Publisher's Note